

---

# Deep Block Proximal Linearised Minimisation Algorithm for Non-convex Inverse Problems

---

**Chaoyan Huang**

The Chinese University of Hong Kong  
cyhuang@math.cuhk.edu.hk

**Zhongming Wu**

NUIST  
wuzm@nuist.edu.cn

**Yanqi Cheng**

University of Cambridge  
yc443@cam.ac.uk

**Tieyong Zeng**

The Chinese University of Hong Kong  
zeng@math.cuhk.edu.hk

**Carola-Bibiane Schönlieb**

University of Cambridge  
cbs31@cam.ac.uk

**Angelica I. Aviles-Rivero**

University of Cambridge  
ai323@cam.ac.uk

## Abstract

Image restoration is typically addressed through non-convex inverse problems, which are often solved using first-order block-wise splitting methods. In this paper, we consider a general type of non-convex optimisation model that captures many inverse image problems and present an inertial block proximal linearised minimisation (iBPLM) algorithm. Our new method unifies the Jacobi-type parallel and the Gauss-Seidel-type alternating update rules, and extends beyond these approaches. The inertial technique is also incorporated into each block-wise sub-problem update, which can accelerate numerical convergence. Furthermore, we extend this framework with a plug-and-play variant (PnP-iBPLM) that integrates deep gradient denoisers, offering a flexible and robust solution for complex imaging tasks. We provide comprehensive theoretical analysis, demonstrating both subsequential and global convergence of the proposed algorithms. To validate our methods, we apply them to multi-block dictionary learning problems in image denoising and deblurring. Experimental results show that both iBPLM and PnP-iBPLM significantly enhance numerical performance and robustness in these applications.

## 1 Introduction

Image processing is crucial in solving a broad spectrum of inverse problems. Over the past decades, a large body of literature has been proposed to address imaging challenges. These range from classic models, such as the Rudin-Osher-Fatemi (ROF) model [41], to modern approaches like dictionary learning [1] and tight frame-based methods [14]. Among these, the dictionary learning paradigm stands out for its ability to approximate clean images ( $I$ ) using dictionaries ( $D$ ) and corresponding sparse coefficient vectors ( $X$ ), effectively framed as  $DX = I$ . However, relying on the  $\ell_0$  norm to maintain sparsity in  $X$  makes this optimisation problem non-convex and involves multiple variables.

Different from other models, the dictionary learning approach aims to approximate the clean image  $I$  using the dictionary  $D$  and the corresponding sparse coefficient vector  $X$ . This leads to the following image denoising model:

$$\min_{D, X} \frac{1}{2} \|DX - Y\|^2 + \lambda_D \phi_D(D) + \lambda_X \phi_X(X), \quad (1)$$

where  $Y$  is the input image,  $\lambda_D$  and  $\lambda_X$  are positive parameters,  $\phi_D$  and  $\phi_X$  are regularisers of  $D$  and  $X$ , respectively. The optimal  $D$  and  $X$  are typically obtained via alternating-based [17] or block-based [58] algorithms. The clean image is then reconstructed by  $DX = I$ . However, this model does not adapt well to other image restoration tasks. To address this, the Bayesian Maximum A Posteriori theory is incorporated to establish a more general model:

$$\min_{D, X, I} \frac{1}{2} \|BI - Y\|^2 + \frac{\eta}{2} \|DX - I\|^2 + \lambda_D \phi_D(D) + \lambda_X \phi_X(X), \quad (2)$$

where  $\eta$  is a positive parameter and  $B$  is a linear operator for different image restoration tasks. For instance, when  $B$  is the identity operator, (2) functions as a denoising model; conversely, when  $B$  is a sampling operator, the model serves as a super-resolution model. Due to the sparsity of the dictionary learning model, detailed information can often mistakenly be treated as noise. To preserve edge details, the works of that [22] and [53] introduced the total variation prior into model (2). Furthermore, various plug-and-play learning priors are utilised to replace the traditional knowledge-based regularisation, introducing inexplicitness and non-convexity into the model. Consequently, existing methods may not efficiently solve these complex models.

The aforementioned non-convex dictionary learning model motivates us to consider the following type of structural non-convex optimisation problem:

$$\min \left\{ F(x_1, \dots, x_p) := \sum_{i=1}^p \theta_i(x_i) + h(x_1, \dots, x_p) \mid x_i \in \mathbb{R}^{n_i} \right\}, \quad (3)$$

where  $h$  is a block-coordinate-wise Lipschitz smooth function and  $\theta_i, i = 1, \dots, p$ , are proper closed (possibly non-convex) functions. The Jacobi-type and the Gauss-Seidel-type block coordinate descent (BCD) methods are two categories of solving methods for (3). Both methods deal with each block-variable  $x_i$  individually in (3). The Jacobi-type methods [18; 38; 59] update the variables in parallel, while the Gauss-Seidel-type algorithms [5; 11; 20; 26] update them alternately, one by one. However, their effectiveness depends on the complexity of solving the block-wise subproblems.

Block-wise subproblems typically involve evaluating the proximal operator [34] of certain functions, which may include total variational (TV) or learning-based regularisation in inverse image problems. However, most of these proximal subproblems lack a closed-form solution, particularly in cases of implicit learning regularisation. Fortunately, the plug-and-play [50] (PnP) method can effectively address this challenge by alternately solving the subproblems using a trained deep neural network.

**Contributions.** To our knowledge, no existing work integrates the Gauss-Seidel-type BCD algorithms with the PnP approach. This paper aims to fill this gap. Additionally, this paper seeks to unify the Jacobi-type and the Gauss-Seidel-type BCD methods within a single algorithmic framework. Furthermore, inertial acceleration is introduced to enhance convergence speed, and the theoretical convergence of the unified algorithm, with or without the PnP prior, is examined. We highlight:

- We introduce a novel general inertial block proximal linearised minimisation (iBPLM) algorithm framework for solving the non-convex and non-smooth optimisation problem of that (3). Our new method synthesises the Jacobi-type parallel and the Gauss-Seidel-type alternating update rules, thereby enhancing performance and properties.
- Secondly, inspired by the principles of the Plug-and-Play (PnP) method, we redefine the iBPLM algorithm as the PnP-iBPLM. This version integrates gradient step-based deep priors. It significantly boosts the algorithm’s ability to tackle more intricate and challenging optimisation problems. As a result, it sets a new standard in algorithm performance and adaptability.
- By employing the Kurdyka–Łojasiewicz property, we have rigorously proved the subsequential and global convergence of both the iBPLM and PnP-iBPLM algorithms. This provides a solid theoretical underpinning, ensuring consistent performance across a range of complex optimisation scenarios.
- We extensively validate the theory with a range of numerical and visual results for image denoising and deblurring tasks. We demonstrate that our framework leads to better approximations than existing techniques.

## 2 Related Work

- **BCD-based Optimisation Algorithms.** Block coordinate descent (BCD) methods are commonly used for imaging problems by updating one block of variables at a time while fixing others. These

Table 1: **Comparative Overview of Existing Techniques.** This table delineates differences in problem settings, algorithm designs, and convergence results. Abbreviations include: Non. (Non-convex), Para. (Parallel), Alter. (Alternating), Iner. (Inertial), PnP (Plug-and-Play), Sub. (Subsequential), and Global (Global convergence).

EXISTING TECHNIQUES	Problem setting		Algorithm design				Theoretical results	
	$h$ Non.	$\theta_i$ Non.	Para.	Alter.	Iner.	PnP	Sub.	Global
(Xu & Yin, 2013) [57]	✓	✗	✗	✓	✓	✗	✓	✓
(Razaviyayn et al., 2014) [38]	✓	✗	✓	✗	✓	✗	✓	✗
(Hong et al., 2017) [21]	✗	✗	✗	✓	✓	✗	✓	✓
(Xu & Yin, 2017) [59]	✓	✓	✓	✗	✓	✗	✓	✓
(Teboulle & Vaisbourd, 2020) [47]	✓	✓	✓	✗	✗	✗	✓	✓
(Hien et al., 2020) [26]	✓	✓	✗	✓	✗	✗	✓	✓
(Yang et al., 2020) [62]	✓	✗	✗	✓	✗	✗	✓	✓
(Sujithra & Sugitha, 2022) [44]	✓	✓	✗	✗	✗	✓	✗	✗
(Phan et al., 2023) [20]	✓	✓	✗	✓	✓	✗	✓	✓
(Gan et al., 2024) [18]	✓	✓	✓	✗	✗	✓	✗	✗
★ Ours	✓	✓	✓	✓	✓	✓	✓	✓

methods can be broadly categorised into two types: alternating-based and block-based. Alternating-based methods, such as the proximal alternating linearised minimisation (PALM) algorithm, update subsets of variables sequentially, effectively merging the benefits of proximal operators with alternating minimisation. PALM is particularly effective for non-smooth and non-convex problems, and it has demonstrated global convergence under specified conditions [11]. Recent studies have further validated its effectiveness and convergence properties in various settings [51; 52]. There are three principal types of block-based methods: classical block-based [49], proximal block-based [37], and proximal gradient block-based [11] methods. The classical block-based method alternates the minimisation of block functions within the objective but may be inadequate for non-convex problems. The proximal block-based method enhances this approach by integrating block functions with a proximal term, thereby ensuring global convergence under specific conditions [5]. The proximal gradient block-based method, on the other hand, minimises a proximal linearisation of the objective and achieves global convergence when block functions are Lipschitz smooth [11]. Moreover, when block functions exhibit relative smoothness, further studies have demonstrated global convergence [9; 28; 3; 19].

- Inertial Acceleration.** Numerous studies have focused on enhancing the convergence rate of gradient-based first-order methods, as demonstrated in [30; 35; 55]. A widely adopted strategy involves incorporating an inertial force, often referred to as extrapolation, into the iterative scheme. This approach leverages the outcomes of the previous two iterations to update the next iterate, ultimately resulting in the development of inertial accelerated methods. Well-known techniques such as the classic heavy-ball method and Nesterov acceleration are exemplary of this type of accelerated method. In convex settings, extensive research has shown that the convergence rate can be theoretically accelerated by selecting optimal extrapolated schemes [8; 7; 10]. Over the past decade, inertial acceleration has been adapted for non-convex optimisation [2; 35; 32; 31; 20; 36; 56], and has been effectively integrated into BCD-based optimisation algorithms [57; 59; 37; 26; 20]. The convergence of these inertial methods to a stationary point can be guaranteed under the Kurdyka–Łojasiewicz framework for non-convex problems [5]. Although the inertial effect may not theoretically accelerate the convergence rate in non-convex settings, numerous practical implementations have demonstrated its effectiveness.

- Plug-and-Play (PnP) Algorithms.** PnP methods integrate denoising priors into splitting algorithms, which are widely used for imaging problems [65]. PnP-ADMM, introduced by Venkatakrishnan et al. [50], replaces the proximal subproblem with a denoising prior, offering a flexible framework for image restoration. Subsequent approaches like PnP-FBS [54] and PnP-DRS [13] have demonstrated empirical success across diverse applications. However, theoretical guarantees are limited, often relying on assumptions such as denoiser averaging or nonexpansiveness [45; 46]. A significant challenge is ensuring nonexpansiveness in deep denoisers, which is crucial for convergence. Off-the-shelf deep denoisers often lack 1-Lipschitz continuity, which affects performance [64]. Ryu et al. [42] proposed normalising each layer using its spectral norm, but this limits residual skip connections. The work of that [24] addressed this by training a denoiser with a gradient-based PnP prior. Recent advancements have led to exploring convergence guarantees

and applying combined PnP methods with extrapolated DYS algorithms [55]. These developments potentially enhance both convergence and applicability in complex inverse problems.

• **Dictionary Learning-based Image Restoration.** Dictionary learning is a powerful technique for image restoration. The goal is to learn a dictionary from given data so that each image patch can be sparsely represented by a linear combination of dictionary atoms. This method is especially effective for inverse problems like image denoising and deblurring. The seminal work by Aharon et al. [1] introduced the K-SVD algorithm. It iteratively refines both the dictionary and the sparse representations, leading to significant improvements in image quality. Subsequent research has expanded on this foundation, exploring various aspects of dictionary learning and sparse coding [14; 17; 29]. Moreover, recent advancements focus on integrating dictionary learning with deep learning techniques. This integration involves learning the dictionary from neural networks [33; 43] or combining it with the PnP method to handle the dictionary learning model [44; 61]. However, most of these studies overlook the theoretical analysis of the dictionary-based model.

The aforementioned methods are primarily encompassed within the framework of problem (3). We detail the most relevant works along with their problem settings, algorithm designs, and theoretical analyses in Table 1. This summary clearly demonstrates that our proposed iBPLM and PnP-iBPLM algorithms comprehensively cover all these aspects, effectively addressing the limitations identified in previous studies and providing a robust, theoretically sound framework for optimisation.

### 3 Proposed Method

This section details our proposed unified inertial block proximal linearised minimisation method and its Plug-and-Play (PnP) variant, along with establishing their theoretical convergence.

**Notation.** Denote  $x_{<i} := (x_1, x_2, \dots, x_{i-1})$ ,  $x_{>i} := (x_{i+1}, x_{i+2}, \dots, x_p)$ , and  $x_{\neq i} := (x_{<i}, x_{>i})$ . The distance between a point  $x \in \mathbb{R}^n$  and a closed and convex set  $\mathcal{G} \subseteq \mathbb{R}^n$  is defined as  $\text{dist}(x, \mathcal{G}) := \min_{y \in \mathcal{G}} \|x - y\|$ . The indicator function for  $\mathcal{G}$  assigns 0 to all  $x \in \mathcal{G}$  and  $+\infty$  otherwise. For  $\gamma > 0$ , the proximal operator of the function  $f$  is defined by  $\text{Prox}_{\gamma f}(x) := \arg \min_{y \in \mathbb{R}^n} \{f(y) + \frac{1}{2\gamma} \|y - x\|^2\}$ .

#### 3.1 Inertial block proximal linearised minimisation algorithm

We first propose an inertial block proximal linearised minimisation (iBPLM) algorithm for solving the non-convex and non-smooth model of that (3), referred to as Algorithm 1. This algorithm can be utilised to handle dictionary learning models with explicit regularisation.

By introducing a weight matrix  $W := (w_{ij})_{p \times p}$ , Algorithm 1 establishes a unified framework. This framework incorporates the Jacobi-type parallel update rule among task blocks, as well as the Gauss-Seidel-type alternating update within each block. Specifically, the matrix  $W$  is employed to compute  $x_j^{k,i}$ , defined as  $x_j^{k,i} = (1 - w_{ij})x_j^{k+1} + w_{ij}x_j^k$  for all  $i, j = 1, 2, \dots, p$ , where  $w_{ij} \in [0, 1]$  for  $j < i$  and  $w_{ij} = 1$  for  $j \geq i$ . When  $w_{ij} = 1$  and  $w_{ij} = 0 \forall j < i$ , the matrix  $W = W_1$  and

---

#### Algorithm 1 Inertial block proximal linearised minimisation algorithm (iBPLM)

---

Initialisation: Select  $w_{ij} \in [0, 1]$  for  $j < i$  and  $w_{ij} = 1$  for  $j \geq i$ . Given  $x_i^0$ , set  $x_i^{-1} = x_i^0$ .

**for**  $k = 1, 2, 3, \dots$  **do**

Update  $x_j^{k,i} = (1 - w_{ij})x_j^{k+1} + w_{ij}x_j^k$ ,  $\forall i, j = 1, 2, \dots, p$ ;

**for**  $i = 1, 2, 3, \dots, p$  **do**

Choosing  $\alpha_i^k \in [0, 1)$ .

Update  $\hat{x}_i^k = x_i^k + \alpha_i^k(x_i^k - x_i^{k-1})$ ;

Update  $x_i^{k+1} = \text{Prox}_{\gamma_i^k \theta_i}(\hat{x}_i^k - \gamma_i^k \nabla_i h(\hat{x}_i^k, x_{\neq i}^{k,i}))$ .

**end for**

**if** stopping criterion is satisfied **then**

Return  $(x_1^k, x_2^k, \dots, x_p^k)$

**end if**

**end for**

---

$W = W_2$  defined by:

$$W_1 = \begin{bmatrix} 1 & 1 & \cdots & 1 \\ 1 & 1 & \cdots & 1 \\ \vdots & \ddots & \ddots & \vdots \\ 1 & \cdots & 1 & 1 \end{bmatrix} \quad \text{and} \quad W_2 = \begin{bmatrix} 1 & 1 & \cdots & 1 \\ 0 & 1 & \cdots & 1 \\ \vdots & \ddots & \ddots & \vdots \\ 0 & \cdots & 0 & 1 \end{bmatrix}, \quad (4)$$

Algorithm 1 simplifies to the Jacobi-type and Gauss-Seidel-type BPLM, respectively. Additionally, to accelerate the convergence of the unified algorithm, an inertial step is incorporated into the updates of the block-subproblems.

Now we begin to analyse the theoretical convergence of iBPLM. To do so, we established the following mild assumption.

**Assumption 1.** *The gradient of  $h$  is block-coordinate-wise Lipschitz continuous; that is, for a given  $x_{\neq i}$ , it holds that*

$$\|\nabla_i h(x_i, x_{\neq i}) - \nabla_i h(y_i, x_{\neq i})\| \leq L_i(x_{\neq i})\|x_i - y_i\|, \text{ for } i = 1, 2, \dots, p.$$

Denote  $L_i^k := L_i(x_{<i}^{k+1}, x_{>i}^k)$ , and  $L^k := \max\{L_i^k, i = 1, 2, \dots, p\}$ . We summarise the property of  $F$  in the following proposition, whose proof can be found in Appendix B.

**Proposition 1.** *For the sequence  $\{x^k\}$  generated by the proposed iBPLM algorithm, it must satisfy*

$$F(x^k) + \sum_{i=1}^p \frac{\xi_i^k}{2} \|x_i^k - x_i^{k-1}\|^2 \geq F(x^{k+1}) + \sum_{i=1}^p \frac{\delta_i^k}{2} \|x_i^{k+1} - x_i^k\|^2, k = 1, 2, \dots \quad (5)$$

where  $\xi_i^k := \frac{\alpha_i^k \gamma_i^k L_i^k + \alpha_i^k}{\gamma_i^k}$ ,  $\delta_i^k := \frac{1 - \alpha_i^k - \gamma_i^k L_i^k - \alpha_i^k \gamma_i^k L_i^k - \gamma_i^k w'_i L_i^k}{\gamma_i^k}$ , and  $w'_i = \sum_{q=i+1}^p w_{qi}$ .

Note that if the sequences  $\{\xi_i^k\}$  and  $\{\delta_i^k\}$  are positive and adhere to certain relationships, the variant of the objective function in (3) is non-increasing with respect to the iteration number  $k$ . The following lemma outlines the parameter conditions; the proof of this result can be found in Appendix C.

**Lemma 1.** *Let  $\{x^k\}$  be the sequence generated by the iBPLM algorithm. If  $\xi_i^{k+1} \leq C\delta_i^k$  for some constant  $C \in (0, 1)$ , and there exists a positive parameter  $\underline{l}$  such that  $\min_{i,k} \{\frac{\delta_i^k}{2}\} \geq \underline{l}$  then we have*

$$\sum_{k=0}^{+\infty} \sum_{i=1}^m \|x_i^{k+1} - x_i^k\|^2 < +\infty. \quad (6)$$

**Remark 1.** *Indeed, it is not difficult to guarantee the parameter condition  $\xi_i^{k+1} \leq C\delta_i^k$ . For instance, if  $W = W_2$  and the parameters are constant such that  $\alpha_i^k = \alpha_i$  and  $\gamma_i^k = \gamma_i$  for all  $k$ , it holds that  $w'_i = 0$ , and the condition  $\xi_i^{k+1} \leq C\delta_i^k$  can be satisfied if*

$$0 < \gamma_i < \frac{1}{L_i}, \quad \text{and} \quad 0 \leq \alpha_i < \frac{1 - \gamma_i L_i}{2 + 2\gamma_i L_i}. \quad (7)$$

Note that in the implementation, as discussed in [27; 60], one can initialise the algorithm with larger values of  $\alpha_i$  and  $\gamma_i$ . If these parameters do not meet the required conditions, they should be decreased by a constant ratio. This adjustment is necessary if the sequence generated by the algorithm becomes unbounded, or if the successive changes in the sequence do not diminish sufficiently fast.

Our first theoretical result concerns the subsequential convergence of the iBPLM to a stationary point of (3). This result is detailed in the following theorem, with the proof available in Appendix D.

**Theorem 1.** *Suppose that Proposition 1 and Lemma 1 hold. Assume that the sequence  $\{x^k\}$  generated by the proposed iBPLM Algorithm is bounded. Every limit point  $x^*$  of  $\{x^k\}$  is a critical point of problem (3).*

We demonstrate the global convergence of iBPLM if the objection function in (3) satisfies the Kurdyka–Łojasiewicz property in the follow theorem, whose proof can be found in Appendix E.

---

**Algorithm 2** Plug-and-play iBPLM algorithm (PnP-iBPLM)

---

Initialisation: Select  $w_{ij} \in [0, 1]$  for  $j < i$  and  $w_{ij} = 1$  for  $j \geq i$ . Given  $x_i^0$ , set  $x_i^{-1} = x_i^0$ .

**for**  $k = 1, 2, 3, \dots$  **do**

  Update  $x_j^{k,i} = (1 - w_{ij})x_j^{k+1} + w_{ij}x_j^k, \quad \forall i, j = 1, 2, \dots, p;$

**for**  $i = 1, 2, 3, \dots, p$  **do**

    Choosing  $\alpha_i^k \in [0, 1)$ .

    Update  $\hat{x}_i^k = x_i^k + \alpha_i^k(x_i^k - x_i^{k-1});$

    Update  $x_i^{k+1} = \mathcal{D}_{\sigma_i}(\hat{x}_i^k - \gamma_i^k \nabla_i h(\hat{x}_i^k, x_{\neq i}^{k,i})).$

**end for**

**if** stopping criterion is satisfied **then**

    Return  $(x_1^k, x_2^k, \dots, x_p^k)$

**end if**

**end for**

---

**Theorem 2.** *Suppose that Proposition 1, Lemma 1, and assumption 2 hold. Assume that the sequence  $\{x^k\}$  generated by the proposed iBPLM Algorithm is bounded. Let  $h$  be a continuously differentiable function,  $F$  is a KL function and together with the existence of  $\underline{l}$  in Lemma 1, we also assume there exists  $\bar{l} > 0$ , such that  $\max_{i,k} \{\frac{\delta_i^k}{2}\} \leq \bar{l}$ . For  $C$  in Proposition 1 satisfying  $C < \underline{l}/\bar{l}$ , the whole generated sequence  $\{x^k\}$  of the proposed iBPLM algorithm is convergent.*

Moreover, if the function  $\psi$  appearing in the KL inequality takes the form  $\psi(s) = cs^{1-\theta}$  with  $\theta \in [0, 1)$  and  $c > 0$ , we can derive the convergence rates for both sequences  $\{x^k\}$  and  $\{F(x^k)\}$ .

**Theorem 3.** *Let  $\{x^k\}$  be a sequence generated by iBPLM. Suppose that Assumptions in Theorem 2 are satisfied. If  $\{x^k\}$  is bounded and the function  $\psi$  appearing in the KL inequality takes the form  $\psi(s) = cs^{1-\theta}$  with  $\theta \in [0, 1)$  and  $c > 0$ , then the following statements hold. (i) If  $\theta = 0$ , the sequences  $\{x^k\}$  and  $\{F(x^k)\}$  converge in a finite number of steps to  $x^*$  and  $F^*$ , respectively. (ii) If  $\theta \in (0, 1/2]$ , the sequences  $\{x^k\}$  and  $\{F(x^k)\}$  converge linearly to  $x^*$  and  $F^*$ , respectively. (iii) If  $\theta \in (1/2, 1)$ , there exist positive constants  $\delta_1, \delta_2$ , and  $N$  such that  $\|x^k - x^*\| \leq \delta_1 k^{\frac{1-\theta}{2\theta-1}}$  and  $F(x^k) - F^* \leq \delta_2 k^{-\frac{1}{2\theta-1}}$  for all  $k \geq N$ .*

Because this theorem can be proven by using the same techniques as those in the proofs of Attouch and Bolte [4, theorem 2], we omit the detail of the proof.

### 3.2 Plug-and-Play iBPLM Algorithm

In this section, we propose the following plug-and-play inertial block proximal linearised minimisation (PnP-iBPLM) algorithm 2 to solve the non-convex optimisation problem (3). Our approach extends the iBPLM algorithm by integrating deep priors as regularisers, enhancing the robustness of the optimisation process.

We update the  $x_i$  ( $i = 1, 2, \dots, p$ )-subproblems using the gradient step Denoiser [16; 55], defined by

$$\mathcal{D}_{\sigma_i} = I - \nabla g_{\sigma_i}, i = 1, 2, \dots, p, \quad (8)$$

which is obtained from a scalar function

$$g_{\sigma_i} = \frac{1}{2} \|x - N_{\sigma_i}(x)\|^2, \quad (9)$$

where the mapping  $N_{\sigma_i}(x)$  is implemented using a differentiable neural network. This enables the explicit computation of  $g_{\sigma_i}$  and ensures that  $g_{\sigma_i}$  has a Lipschitz gradient with a constant  $L$  (where  $L < 1$ ). Originally, the denoiser  $\mathcal{D}_{\sigma_i}$ , described in (8), is trained to denoise images degraded by Gaussian noise of level  $\sigma_i$ . Notably, the denoiser  $\mathcal{D}_{\sigma_i}$  takes the form of a proximal mapping of a weakly convex function, as detailed in the next proposition.

**Proposition 2** ([55], Proposition 4.1).  $\mathcal{D}_{\sigma_i}(x) = \text{prox}_{\phi_{\sigma_i}}(x)$ , where  $\phi_{\sigma_i}$  is defined by

$$\phi_{\sigma_i}(x) = g_{\sigma_i}(\mathcal{D}_{\sigma_i}^{-1}(x)) - \frac{1}{2} \|\mathcal{D}_{\sigma_i}^{-1}(x) - x\|^2, i = 1, 2, \dots, p, \quad (10)$$

if  $x \in \text{Im}(\mathcal{D}_{\sigma_i})$ , and  $\phi_{\sigma_i}(x) = +\infty$  otherwise. Moreover,  $\phi_{\sigma_i}$  is  $\frac{L}{L+1}$ -weakly convex and  $\nabla\phi_{\sigma_i}$  is  $\frac{L}{1-L}$ -Lipschitz on  $\text{Im}(\mathcal{D}_{\sigma_i})$ , and  $\phi_{\sigma_i}(x) \geq g_{\sigma_i}(x), \forall x \in \mathbb{R}^n$ .

In the following, we present the convergence results of PnP-iBPLM Algorithm.

**Theorem 4.** Let  $g_{\sigma_i} : \mathbb{R}^n \rightarrow \mathbb{R} \cup \{+\infty\}$  of class  $\mathcal{C}^2$  with  $L$ -Lipschitz continuous gradient with  $L < 1$ , and  $\mathcal{D}_{\sigma_i} = I - \nabla g_{\sigma_i}$  and  $h$  is a lower semi-continuous function. Suppose that  $h$  and  $g_{\sigma_i}$  are bounded from below, then the sequence  $\{x^k\}$  generated by the proposed PnP-iBPLM Algorithm, which is assumed to be bounded,

(i) For positive parameters  $\xi_i^k$  and  $\delta_i^k$  satisfy  $\xi_i^{k+1} \leq C\delta_i^k$  for some constant  $C \in (0, 1)$ , we know that with  $\theta_i := \phi_{\sigma_i}$ , the following holds

$$F(x^k) + \sum_{i=1}^p \frac{\xi_i^k}{2} \|x_i^k - x_i^{k-1}\|^2 \geq F(x^{k+1}) + \sum_{i=1}^p \frac{\delta_i^k}{2} \|x_i^{k+1} - x_i^k\|^2, k = 0, 1, \dots \quad (11)$$

(ii) If there exists a positive parameter  $\underline{l}$  such that  $\min_{i,k} \{\frac{\delta_i^k}{2}\} \geq \underline{l}$ , then we have

$$\sum_{k=0}^{+\infty} \sum_{i=1}^m \|x_i^{k+1} - x_i^k\|^2 < +\infty. \quad (12)$$

(iii) Every limit point  $x^*$  of  $\{x^k\}$  is a critical point.

(iv) Assume assumption 2 hold. Let  $F$  be a KL function and together with the existence of  $\underline{l}$  in Lemma 1, we also assume there exists  $\bar{l} > 0$ , such that  $\max_{i,k} \{\frac{\delta_i^k}{2}\} \leq \bar{l}$ . For  $C$  in Proposition 1 satisfying  $C < \underline{l}/\bar{l}$ , the whole generated sequence  $\{x^k\}$  of the proposed PnP-iBPLM algorithm is convergent.

*Proof.* The PnP-iBPLM algorithm is a special case of the problem in (3) with  $\theta_i = \phi_{\sigma_i}$  with given assumptions. Therefore, it follows from Proposition 1, (i) holds; from Lemma 1 that (ii) holds; and from Theorem 1 that (iii) is confirmed. Conclusion (iv) can be derived from Lemma 2 and Theorem 2. This completes the proof.  $\square$

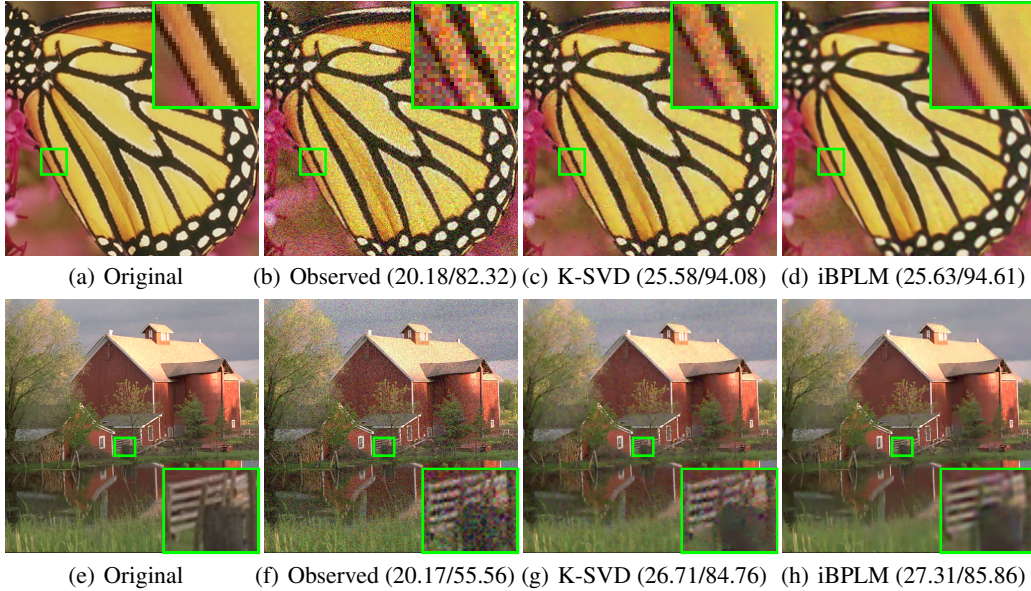


Figure 1: Image restoration results (PSNR/SSIM) with Gaussian noise level 25. Visualisation comparing our technique with K-SVD [40], with two examples presented in (a)-(d) and (e)-(h), respectively.

**Remark 2.** Note that in the implementation, we can select part of the subproblems solved by the gradient-step denoiser, leading to hybrid methods. Furthermore, according to [23, Lemma 1],  $\phi_{\sigma_i}(x)$  in (10) satisfies the Kurdyka-Łojasiewicz (KL) property if  $g_{\sigma_i}$  is real analytic [25] in a neighborhood of  $x \in \mathbb{R}^n$  and its Jacobian matrix  $Jg_{\sigma_i}(x)$  is nonsingular. The analytic nature of  $g_{\sigma_i}$  can be assured for a wide range of deep neural networks. Additionally, the nonsingularity of  $Jg_{\sigma_i}(x)$  can be guaranteed by assuming  $L < 1$  as discussed in [23]. For more discussions on general conditions under which the KL property holds for deep neural networks, we refer to [15; 63]. Therefore, selecting a neural network for  $g_{\sigma_i}$  that guarantees the KL property of  $\phi_{\sigma_i}(x)$  during implementation is attainable.

## 4 Experimental Results

We validate our proposed iBPLM and PnP-iBPLM algorithms on two inverse problem tasks: image denoising and image restoration. We test the algorithms using two blocks in the image denoising task and four blocks in the image restoration task, *both employing dictionary learning-based models*. Following standard protocol, we use two widely recognised metrics: Peak Signal to Noise Ratio (PSNR) and Structural Similarity Index (SSIM). All experiments in this section were run using PyTorch on an NVIDIA RTX A6000 GPU.

### 4.1 iBPLM for Image Denoising

For the specific inverse problem (1), following the proposed iBPLM algorithm, we set  $h(D, X) = \frac{1}{2}\|DX - Y\|^2$ ,  $\theta_X(X) = \lambda_X\|X\|_0$ , and  $\theta_D(D) = \lambda_D\|D\|^2$ . This definition is consistent with the traditional dictionary learning, enabling the dictionary learning denoising model to be solved using our iBPLM algorithm. We start by comparing our technique against that of K-SVD [40].

Table 2: Denoising results of the proposed framework with  $\tau_X = 0.5$ , and K-SVD for noise levels  $\sigma = [25, 50, 75, 100]$ .

NOISE	METRIC	DEGRADED	K-SVD [40]	★iBPLM
$\sigma = 25$	PSNR	20.18	25.58	25.61
	SSIM	82.32	94.08	94.60
$\sigma = 50$	PSNR	14.16	21.27	22.91
	SSIM	59.75	86.64	89.73
$\sigma = 75$	PSNR	10.64	18.79	20.17
	SSIM	42.64	79.31	82.20
$\sigma = 100$	PSNR	8.14	17.38	17.92
	SSIM	30.84	73.61	73.78

Table 2 provides a comparative analysis of denoising performance between the well-established K-SVD method and our proposed iBPLM framework (with  $\tau_X = 0.5$ ) across a range of noise levels. This analysis underscores the iBPLM framework’s superior performance in enhancing both PSNR and SSIM metrics across all tested scenarios. Furthermore, some detailed analysis of weight parameter  $\tau_X$  and inertial parameters  $\alpha_D$  and  $\alpha_X$  are provided in Appendix F. At the lower noise level of  $\sigma = 25$ , the iBPLM not only improves upon the ‘Degraded’ baseline but also edges out K-SVD in SSIM, showcasing its acute capability to preserve image structural integrity even in subtler noise environments. As noise levels escalate, the resilience of iBPLM becomes even more apparent; it consistently records higher SSIM values than K-SVD, which points to its robust ability to maintain visual quality and textural details under more severe noise conditions. This trend holds true even at the very high noise setting of  $\sigma = 100$ , where iBPLM continues to deliver superior structural preservation as indicated by its higher SSIM scores. The consistent outperformance of iBPLM across various noise intensities highlights its potential as a particularly effective tool for applications demanding high fidelity image restoration.

The visual results in Figure 1 further support our framework iBPLM framework in preserving detail and enhancing image quality compared to K-SVD. For the butterfly image, iBPLM restores intricate wing patterns with greater clarity and less noise, as indicated by the higher PSNR and SSIM scores. In the house image, iBPLM demonstrates its strength in rendering architectural details and textures more sharply, particularly in areas such as the roof and surrounding foliage. These images visually support the numerical findings, showing iBPLM’s superior performance in reducing noise while maintaining the integrity of the original images.



Table 3: Average PSNR (dB) and SSIM (%) results of different restoration models for MB(20, 60)/ $\sigma = 25$ . We refer to 'Equivariant' as 'Equi.', and denote our approach with a  $\star$ .

Datasets	Metric	Degraded	DPIR [64]	DiffPIR [66]	Equi. [48]	SNORE [39]	DYSdiff [55]	$\star$ PnP-iBPLM
Set3C	PSNR	14.75	20.78	20.64	22.82	22.14	22.67	23.05
	SSIM	50.85	84.67	85.41	90.68	86.95	89.46	90.71
CBSD10	PSNR	17.58	24.14	23.24	24.74	24.01	24.51	24.77
	SSIM	31.08	74.27	70.97	75.70	70.91	74.94	76.17
Set17	PSNR	17.79	24.16	22.76	24.65	24.17	24.46	24.74
	SSIM	42.20	77.75	73.86	80.42	77.08	79.88	80.85
Set18	PSNR	18.21	25.56	22.86	26.25	25.51	26.03	26.22
	SSIM	51.49	83.76	79.47	87.94	84.15	86.81	87.50
Kodak24	PSNR	18.24	24.99	24.23	25.25	24.70	25.16	25.50
	SSIM	36.30	79.97	77.51	81.19	75.73	79.79	81.03

## 4.2 PnP-iBPLM for Image Restoration

For this specific inverse problem, given the input image  $Y$  with some linear operator  $B$ , the image restoration model can be formulated as follows:

$$\min_{X,D,I,Z} \frac{\eta}{2} \|DX - I\|^2 + \frac{\beta}{2} \|I - Z\|^2 + \lambda_X \phi_X(X) + \lambda_D \phi_D(D) + \lambda_Z \phi_Z(Z) + \frac{\lambda_I}{2} \|BI - Y\|^2, \quad (13)$$

where  $D$  is the dictionary,  $X$  is the corresponding sparse coefficient,  $I$  is the latent image, and  $\eta$ ,  $\beta$ ,  $\lambda_X$ ,  $\lambda_D$ ,  $\lambda_Z$  and  $\lambda_I$  are positive parameters. The  $\phi_D$ ,  $\phi_X$ , and  $\phi_Z$  serve as regularisers for  $D$ ,  $X$ ,  $Z$ , respectively. Following the proposed PnP-iBPLM algorithm, this model can be solved by setting  $h(X, D, I, Z) = \frac{\eta}{2} \|DX - I\|^2 + \frac{\beta}{2} \|I - Z\|^2$ ,  $\theta_X = \lambda_X \phi_X(X)$ ,  $\theta_D = \lambda_D \phi_D(D)$ ,  $\theta_I = \frac{\lambda_I}{2} \|BI - Y\|^2$ ,  $\theta_Z = \lambda_Z \phi_Z(Z)$ . The detailed settings of the dictionary learning image restoration model are provided in Appendix F.

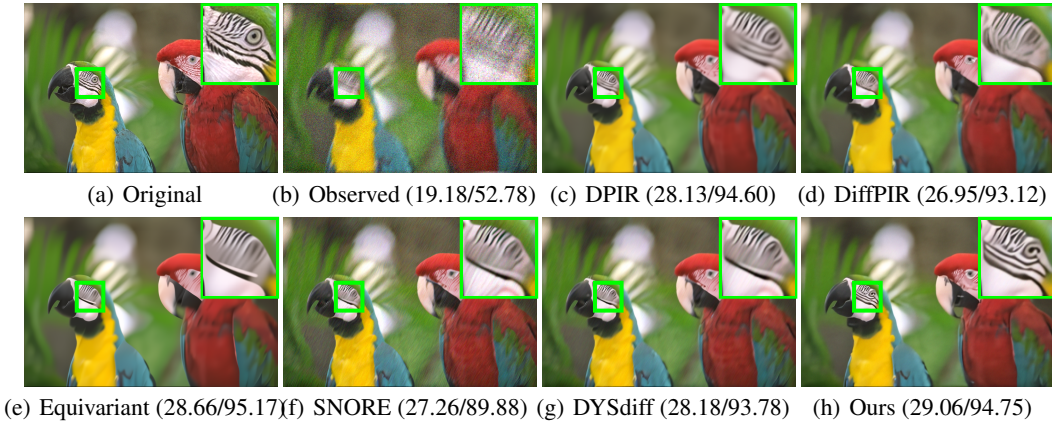


Figure 2: Image restoration results (PSNR/SSIM) with motion blur kernel MB(20, 60) and Gaussian noise level 25. Visualisation comparison of our scheme and some state-of-the-art PnP-based methods: (c) DPIR [64], (d) DiffPIR [66], (e) Equivariant [48], (f) SNORE [39], (g) DYSdiff [55], and (h) Our PnP-iBPLM.

We begin by comparing our proposed PnP-iBPLM against the exiting techniques of that DPIR [64], DiffPIR [66], Equivariant [48], SNORE [39], DYSdiff [55]. Table 3 illustrates the performance of our proposed PnP-iBPLM technique across various datasets at a noise level of  $\sigma$ , comparing favorably with established restoration models like DPIR, DiffPIR, Equivariant, and SNORE. Notably, PnP-iBPLM consistently achieves top-tier SSIM scores, supporting its exceptional capability in preserving image structure and texture, particularly evident in the CBSD10, Set17, and Kodak24 datasets where it leads with the highest SSIM values. While its PSNR scores are occasionally outperformed by the Equivariant model, PnP-iBPLM demonstrates robust overall effectiveness in PSNR as well, especially highlighted in Set18 and Kodak24. This performance underscores the algorithm's

utility in producing high-quality restorations across different types of images and conditions, confirming its adaptability and strength in handling complex noise levels and various degradation types.

The visual results depicted in Figure 2 further support the quantitative findings discussed earlier, affirming the superior performance of PnP-iBPLM in image restoration tasks. Clear and crisp details are preserved in the denoised images produced by PnP-iBPLM, showcasing its ability to effectively remove noise while retaining essential image features. Comparative analysis against existing techniques such as DPIP, DiffPIP, Equivariant, SNORE, and DYSDiff further solidifies PnP-iBPLM’s position as a state-of-the-art solution for high-fidelity image restoration.

## 5 Conclusion

In this paper, we proposed the inertial block proximal linearised minimisation (iBPLM) algorithm, a novel framework for effectively solving non-convex inverse problems in image processing. Addressing the limitations of existing optimisation algorithms, our approach bridges the gap between block-based and alternating-based methods, combining their strengths while mitigating their weaknesses. By integrating extrapolation techniques and deep denoisers within the framework, our PnP-iBPLM algorithm demonstrates robustness and effectiveness in handling non-convex and non-smooth problems, supported by theoretical analysis. Our work contributes significantly to the fields of optimisation and image processing, providing a novel solution for non-convex inverse problems. The superior performance of the iBPLM and PnP-iBPLM algorithms in image denoising and restoration tasks underscores their potential for a wide range of applications.

## Acknowledgments and Disclosure of Funding

ZW acknowledges support from the National Natural Science Foundation of China grant 12001286 and the China Postdoctoral Science Foundation grants 2022M711672. YC acknowledges funding from the Cambridge Centre for Data-Driven Discovery and Accelerate Programme for Scientific Discovery, made possible by a donation from Schmidt Futures. TZ acknowledges support from the NSFC/RGC N\_CUHK 415/19, ITF ITS/173/22FP, RGC 14300219, 14302920, 14301121, and CUHK Direct Grant for Research. CBS acknowledges support from the Philip Leverhulme Prize, the Royal Society Wolfson Fellowship, the EPSRC advanced career fellowship EP/V029428/1, EPSRC grants EP/S026045/1 and EP/T003553/1, EP/N014588/1, EP/T017961/1, the Wellcome Innovator Awards 215733/Z/19/Z and 221633/Z/20/Z, CCMi and the Alan Turing Institute. AAR gratefully acknowledges funding from the Cambridge Centre for Data-Driven Discovery and Accelerate Programme for Scientific Discovery, made possible by a donation from Schmidt Futures, ESRC Digital Core Capability Award, and CMIH and CCIMI, University of Cambridge.

## References

- [1] Michal Aharon, Michael Elad, and Alfred Bruckstein. K-SVD: An algorithm for designing overcomplete dictionaries for sparse representation. *IEEE Transactions on Signal Processing*, 54(11):4311–4322, 2006. 1, 4
- [2] Masoud Ahookhosh, Le Thi Khanh Hien, Nicolas Gillis, and Panagiotis Patrinos. A block inertial Bregman proximal algorithm for nonsmooth nonconvex problems with application to symmetric nonnegative matrix tri-factorization. *Journal of Optimization Theory and Applications*, 190(1):234–258, 2021. 3
- [3] Masoud Ahookhosh, Le Thi Khanh Hien, Nicolas Gillis, and Panagiotis Patrinos. Multi-block Bregman proximal alternating linearized minimization and its application to orthogonal non-negative matrix factorization. *Computational Optimization and Applications*, 79(3):681–715, 2021. 3
- [4] Hedy Attouch and Jérôme Bolte. On the convergence of the proximal algorithm for nonsmooth functions involving analytic features. *Mathematical Programming*, 116:5–16, 2009. 6
- [5] Hedy Attouch, Jérôme Bolte, Patrick Redont, and Antoine Soubeyran. Proximal alternating minimization and projection methods for nonconvex problems: An approach based on the

- kurdyka-łojasiewicz inequality. *Mathematics of Operations Research*, 35(2):438–457, 2010. [2](#), [3](#), [15](#)
- [6] Hedy Attouch, Jérôme Bolte, and Benar Fux Svaiter. Convergence of descent methods for semi-algebraic and tame problems: proximal algorithms, forward–backward splitting, and regularized Gauss–Seidel methods. *Mathematical Programming*, 137(1):91–129, 2013. [15](#)
- [7] Hedy Attouch, Zaki Chbani, Juan Peypouquet, and Patrick Redont. Fast convergence of inertial dynamics and algorithms with asymptotic vanishing viscosity. *Mathematical Programming*, 168:123–175, 2018. [3](#)
- [8] Hedy Attouch and Juan Peypouquet. The rate of convergence of Nesterov’s accelerated forward-backward method is actually faster than  $1/k^2$ . *SIAM Journal on Optimization*, 26(3):1824–1834, 2016. [3](#)
- [9] Heinz H Bauschke, Jérôme Bolte, and Marc Teboulle. A descent lemma beyond lipschitz gradient continuity: First-order methods revisited and applications. *Mathematics of Operations Research*, 42(2):330–348, 2017. [3](#)
- [10] Amir Beck and Marc Teboulle. A fast iterative shrinkage-thresholding algorithm for linear inverse problems. *SIAM Journal on Imaging Sciences*, 2(1):183–202, 2009. [3](#)
- [11] Jérôme Bolte, Shoham Sabach, and Marc Teboulle. Proximal alternating linearized minimization for nonconvex and nonsmooth problems. *Mathematical Programming*, 146(1):459–494, 2014. [2](#), [3](#)
- [12] Jérôme Bolte, Shoham Sabach, and Marc Teboulle. Proximal alternating linearized minimization for nonconvex and nonsmooth problems. *Mathematical Programming*, 146(1-2):459–494, 2014. [15](#)
- [13] Gregory T Buzzard, Stanley H Chan, Suhas Sreehari, and Charles A Bouman. Plug-and-play unplugged: Optimization-free reconstruction using consensus equilibrium. *SIAM Journal on Imaging Sciences*, 11(3):2001–2020, 2018. [3](#)
- [14] Jian-Feng Cai, Raymond H Chan, and Zuowei Shen. A framelet-based image inpainting algorithm. *Applied and Computational Harmonic Analysis*, 24(2):131–149, 2008. [1](#), [4](#)
- [15] Camille Castera, Jérôme Bolte, Cédric Févotte, and Edouard Pauwels. An inertial Newton algorithm for deep learning. *The Journal of Machine Learning Research*, 22(1):5977–6007, 2021. [8](#)
- [16] Regev Cohen, Yochai Blau, Daniel Freedman, and Ehud Rivlin. It has potential: Gradient-driven denoisers for convergent solutions to inverse problems. *Advances in Neural Information Processing Systems*, 34:18152–18164, 2021. [6](#)
- [17] Michael Elad and Michal Aharon. Image denoising via sparse and redundant representations over learned dictionaries. *IEEE Transactions on Image Processing*, 15(12):3736–3745, 2006. [2](#), [4](#)
- [18] Weijie Gan, Yuyang Hu, Jiaming Liu, Hongyu An, Ulugbek Kamilov, et al. Block coordinate plug-and-play methods for blind inverse problems. *Advances in Neural Information Processing Systems*, 36, 2024. [2](#), [3](#)
- [19] Le Thi Khanh Hien and Nicolas Gillis. Algorithms for nonnegative matrix factorization with the Kullback–Leibler divergence. *Journal of Scientific Computing*, 87(3):93, 2021. [3](#)
- [20] Le Thi Khanh Hien, Duy Nhat Phan, and Nicolas Gillis. An inertial block majorization minimization framework for nonsmooth nonconvex optimization. *Journal of Machine Learning Research*, 24(18):1–41, 2023. [2](#), [3](#), [17](#)
- [21] Mingyi Hong, Xiangfeng Wang, Meisam Razaviyayn, and Zhi-Quan Luo. Iteration complexity analysis of block coordinate descent methods. *Mathematical Programming*, 163:85–114, 2017. [3](#)

- [22] Chaoyan Huang, Michael K Ng, Tingting Wu, and Tiejong Zeng. Quaternion-based dictionary learning and saturation-value total variation regularization for color image restoration. *IEEE Transactions on Multimedia*, 24:3769–3781, 2021. 2
- [23] Samuel Hurault, Antonin Chambolle, Arthur Leclaire, and Nicolas Papadakis. Convergent Plug-and-Play with proximal denoiser and unconstrained regularization parameter. *arXiv preprint arXiv:2311.01216*, 2023. 8
- [24] Samuel Hurault, Arthur Leclaire, and Nicolas Papadakis. Gradient step denoiser for convergent plug-and-play. In *International Conference on Learning Representations*, 2022. 3, 21
- [25] Steven G Krantz and Harold R Parks. *A primer of real analytic functions*. Springer Science & Business Media, 2002. 8
- [26] Hien Le, Nicolas Gillis, and Panagiotis Patrinos. Inertial block proximal methods for non-convex non-smooth optimization. In *International Conference on Machine Learning*, pages 5671–5681. PMLR, 2020. 2, 3, 17
- [27] Guoyin Li and Ting Kei Pong. Douglas–Rachford splitting for nonconvex optimization with application to nonconvex feasibility problems. *Mathematical Programming*, 159:371–401, 2016. 5
- [28] Haihao Lu, Robert M Freund, and Yurii Nesterov. Relatively smooth convex optimization by first-order methods, and applications. *SIAM Journal on Optimization*, 28(1):333–354, 2018. 3
- [29] Julien Mairal, Francis Bach, Jean Ponce, and Guillermo Sapiro. Online dictionary learning for sparse coding. In *Proceedings of the 26th Annual International Conference on Machine Learning*, pages 689–696, 2009. 4
- [30] Yu Nesterov. Gradient methods for minimizing composite functions. *Mathematical Programming*, 140(1):125–161, 2013. 3
- [31] Peter Ochs. Unifying abstract inexact convergence theorems and block coordinate variable metric iPiano. *SIAM Journal on Optimization*, 29(1):541–570, 2019. 3
- [32] Peter Ochs, Yunjin Chen, Thomas Brox, and Thomas Pock. iPiano: Inertial proximal algorithm for nonconvex optimization. *SIAM Journal on Imaging Sciences*, 7(2):1388–1419, 2014. 3
- [33] Vardan Pappyan, Yaniv Romano, Jeremias Sulam, and Michael Elad. Convolutional dictionary learning via local processing. In *Proceedings of the IEEE International Conference on Computer Vision*, pages 5296–5304, 2017. 4
- [34] Neal Parikh, Stephen Boyd, et al. Proximal algorithms. *Foundations and Trends® in Optimization*, 1(3):127–239, 2014. 2
- [35] Thomas Pock and Shoham Sabach. Inertial proximal alternating linearized minimization (ipalm) for nonconvex and nonsmooth problems. *SIAM Journal on Imaging Sciences*, 9(4):1756–1787, 2016. 3
- [36] Yunfei Qu, Hongjin He, and Deren Han. A partially inertial customized Douglas–Rachford splitting method for a class of structured optimization problems. *Journal of Scientific Computing*, 98(1):9, 2024. 3
- [37] Meisam Razaviyayn, Mingyi Hong, and Zhi-Quan Luo. A unified convergence analysis of block successive minimization methods for nonsmooth optimization. *SIAM Journal on Optimization*, 23(2):1126–1153, 2013. 3
- [38] Meisam Razaviyayn, Mingyi Hong, Zhi-Quan Luo, and Jong-Shi Pang. Parallel successive convex approximation for nonsmooth nonconvex optimization. *Advances in Neural Information Processing Systems*, 27, 2014. 2, 3
- [39] Marien Renaud, Jean Prost, Arthur Leclaire, and Nicolas Papadakis. Plug-and-play image restoration with stochastic denoising regularization. *arXiv preprint arXiv:2402.01779*, 2024. 9, 20, 21, 22, 23, 24

- [40] Ron Rubinstein, Tomer Peleg, and Michael Elad. Analysis k-svd: A dictionary-learning algorithm for the analysis sparse model. *IEEE Transactions on Signal Processing*, 61(3):661–677, 2012. 7, 8
- [41] Leonid I Rudin, Stanley Osher, and Emad Fatemi. Nonlinear total variation based noise removal algorithms. *Physica D: Nonlinear Phenomena*, 60(1-4):259–268, 1992. 1
- [42] Ernest Ryu, Jialin Liu, Sicheng Wang, Xiaohan Chen, Zhangyang Wang, and Wotao Yin. Plug-and-play methods provably converge with properly trained denoisers. In *International Conference on Machine Learning*, pages 5546–5557. PMLR, 2019. 3
- [43] Meyer Scetbon, Michael Elad, and Peyman Milanfar. Deep k-svd denoising. *IEEE Transactions on Image Processing*, 30:5944–5955, 2021. 4
- [44] MS Sujithra and N Sugitha. Compressed image restoration by combining trained dictionary with plug and play framework. *Wireless Personal Communications*, 124(4):2809–2829, 2022. 3, 4
- [45] Yu Sun, Brendt Wohlberg, and Ulugbek S Kamilov. An online plug-and-play algorithm for regularized image reconstruction. *IEEE Transactions on Computational Imaging*, 5(3):395–408, 2019. 3
- [46] Yu Sun, Zihui Wu, Xiaojian Xu, Brendt Wohlberg, and Ulugbek S Kamilov. Scalable plug-and-play admm with convergence guarantees. *IEEE Transactions on Computational Imaging*, 7:849–863, 2021. 3
- [47] Marc Teboulle and Yakov Vaisbourd. Novel proximal gradient methods for nonnegative matrix factorization with sparsity constraints. *SIAM Journal on Imaging Sciences*, 13(1):381–421, 2020. 3
- [48] Matthieu Terris, Thomas Moreau, Nelly Pustelnik, and Julian Tachella. Equivariant plug-and-play image reconstruction. In *Proceedings of the IEEE/CVF Conference on Computer Vision and Pattern Recognition*, 2024. 9, 20, 21, 22, 23, 24
- [49] Paul Tseng. Convergence of a block coordinate descent method for nondifferentiable minimization. *Journal of Optimization Theory and Applications*, 109:475–494, 2001. 3
- [50] Singanallur V Venkatakrishnan, Charles A Bouman, and Brendt Wohlberg. Plug-and-play priors for model based reconstruction. In *2013 IEEE Global Conference on Signal and Information Processing*, pages 945–948. IEEE, 2013. 2, 3
- [51] Peng Wang, Huikang Liu, and Anthony Man-Cho So. Linear convergence of a proximal alternating minimization method with extrapolation for-norm principal component analysis. *SIAM Journal on Optimization*, 33(2):684–712, 2023. 3
- [52] Qingsong Wang and Deren Han. Stochastic Gauss–Seidel type inertial proximal alternating linearized minimization and its application to proximal neural networks. *Mathematical Methods of Operations Research*, pages 1–36, 2024. 3
- [53] Tingting Wu, Chaoyan Huang, Zhengmeng Jin, Zhigang Jia, and Michael K Ng. Total variation based pure quaternion dictionary learning method for color image denoising. *International Journal of Numerical Analysis & Modeling*, 19(5), 2022. 2
- [54] Tingting Wu, Wei Li, Shilong Jia, Yiqiu Dong, and Tiejong Zeng. Deep multi-level wavelet-CNN denoiser prior for restoring blurred image with Cauchy noise. *IEEE Signal Processing Letters*, 27:1635–1639, 2020. 3
- [55] Zhongming Wu, Chaoyan Huang, and Tiejong Zeng. Extrapolated plug-and-play three-operator splitting methods for nonconvex optimization with applications to image restoration. *arXiv preprint arXiv:2403.01144*, 2024. 3, 4, 6, 9, 20, 21, 22, 23, 24
- [56] Zhongming Wu and Min Li. General inertial proximal gradient method for a class of nonconvex nonsmooth optimization problems. *Computational Optimization and Applications*, 73:129–158, 2019. 3

- [57] Yangyang Xu and Wotao Yin. A block coordinate descent method for regularized multiconvex optimization with applications to nonnegative tensor factorization and completion. *SIAM Journal on Imaging Sciences*, 6(3):1758–1789, 2013. 3
- [58] Yangyang Xu and Wotao Yin. A fast patch-dictionary method for whole image recovery. *Inverse Problems and Imaging*, 10(2):563–583, 2016. 2
- [59] Yangyang Xu and Wotao Yin. A globally convergent algorithm for nonconvex optimization based on block coordinate update. *Journal of Scientific Computing*, 72(2):700–734, 2017. 2, 3
- [60] Lei Yang, Ting Kei Pong, and Xiaojun Chen. Alternating direction method of multipliers for a class of nonconvex and nonsmooth problems with applications to background/foreground extraction. *SIAM Journal on Imaging Sciences*, 10(1):74–110, 2017. 5
- [61] Qing Yang and Yaping Zhao. Revisit dictionary learning for video compressive sensing under the plug-and-play framework. In *Seventh Asia Pacific Conference on Optics Manufacture and 2021 International Forum of Young Scientists on Advanced Optical Manufacturing (APCOM and YSAOM 2021)*, volume 12166, pages 2018–2025. SPIE, 2022. 4
- [62] Yang Yang, Marius Pesavento, Zhi-Quan Luo, and Björn Ottersten. Inexact block coordinate descent algorithms for nonsmooth nonconvex optimization. *IEEE Transactions on Signal Processing*, 16:947–961, 2020. 3
- [63] Jinshan Zeng, Tim Tsz-Kit Lau, Shaobo Lin, and Yuan Yao. Global convergence of block coordinate descent in deep learning. In *International Conference on Machine Learning*, pages 7313–7323. PMLR, 2019. 8
- [64] Kai Zhang, Yawei Li, Wangmeng Zuo, Lei Zhang, Luc Van Gool, and Radu Timofte. Plug-and-play image restoration with deep denoiser prior. *IEEE Transactions on Pattern Analysis and Machine Intelligence*, 44(10):6360–6376, 2021. 3, 9, 20, 21, 22, 23, 24
- [65] Kai Zhang, Wangmeng Zuo, Shuhang Gu, and Lei Zhang. Learning deep CNN denoiser prior for image restoration. In *Proceedings of the IEEE Conference on Computer Vision and Pattern Recognition*, pages 3929–3938, 2017. 3
- [66] Yuanzhi Zhu, Kai Zhang, Jingyun Liang, Jiezhong Cao, Bihan Wen, Radu Timofte, and Luc Van Gool. Denoising diffusion models for plug-and-play image restoration. In *Proceedings of the IEEE/CVF Conference on Computer Vision and Pattern Recognition*, pages 1219–1229, 2023. 9, 20, 21, 22, 23, 24

## A Preliminary

We review the definitions of subdifferential and Kurdyka-Łojasiewicz (KL) property for further analysis.

**Definition 1.** [6; 12] (Subdifferentials) Let  $f : \mathbb{R}^n \rightarrow (-\infty, +\infty]$  be a proper and lower semicontinuous function.

- (i) For a given  $x \in \text{dom}f$ , the Fréchet subdifferential of  $f$  at  $x$ , written by  $\widehat{\partial}f(x)$ , is the set of all vectors  $u \in \mathbb{R}^n$  satisfying

$$\liminf_{y \neq x, y \rightarrow x} \frac{f(y) - f(x) - \langle u, y - x \rangle}{\|y - x\|} \geq 0,$$

and we set  $\widehat{\partial}f(x) = \emptyset$  when  $x \notin \text{dom}f$ .

- (ii) The limiting-subdifferential, or simply the subdifferential, of  $f$  at  $x$ , written by  $\partial f(x)$ , is defined by

$$\partial f(x) := \{u \in \mathbb{R}^n \mid \exists x^k \rightarrow x, \text{ s.t. } f(x^k) \rightarrow f(x) \text{ and } \widehat{\partial}f(x^k) \ni u^k \rightarrow u\}. \quad (14)$$

- (iii) A point  $x^*$  is called (limiting-)critical point or stationary point of  $f$  if it satisfies  $0 \in \partial f(x^*)$ , and the set of critical points of  $f$  is denoted by  $\text{crit}f$ .

Next, we recall the KL property [5; 12], which is important in the convergence analysis.

**Definition 2.** (KL property and KL function) Let  $f : \mathbb{R}^n \rightarrow (-\infty, +\infty]$  be a proper and lower semicontinuous function.

- (a) The function  $f$  is said to have KL property at  $x^* \in \text{dom}(\partial f)$  if there exist  $\eta \in (0, +\infty]$ , a neighborhood  $U$  of  $x^*$  and a continuous and concave function  $\varphi : [0, \eta) \rightarrow \mathbb{R}_+$  such that

- (i)  $\varphi(0) = 0$  and  $\varphi$  is continuously differentiable on  $(0, \eta)$  with  $\varphi' > 0$ ;  
(ii) for all  $x \in U \cap \{z \in \mathbb{R}^n \mid f(x^*) < f(z) < f(x^*) + \eta\}$ , the following KL inequality holds:

$$\varphi'(f(x) - f(x^*)) \text{dist}(0, \partial f(x)) \geq 1. \quad (15)$$

- (b) If  $f$  satisfies the KL property at each point of  $\text{dom}(\partial f)$ , then  $f$  is called a KL function.

**Remark 3.** KL functions exhibit remarkable versatility and are extensively applied in various domains, including semi-algebraic analysis, subanalytic analysis, and log-exp functions. Concrete examples of KL functions can be found in [5; 6; 12]. These examples encompass many common instances such as  $\ell_p$ -norm (where  $p \geq 0$ ), indicator functions of semi-algebraic sets, and a majority of convex functions.

## B Proof of Proposition 1

*Proof.* It follows from Algorithm 1 that

$$x_i^{k+1} = \arg \min_{x_i} \left\{ \langle x_i - \hat{x}_i^k, \nabla_i h(\hat{x}_i^k, x_{\neq i}^{k,i}) \rangle + \frac{1}{2\gamma_i^k} \|x_i - \hat{x}_i^k\|^2 + \theta_i(x_i) \right\},$$

which implies that

$$\begin{aligned} & \langle x_i^k - \hat{x}_i^k, \nabla_i h(\hat{x}_i^k, x_{\neq i}^{k,i}) \rangle + \frac{1}{2\gamma_i^k} \|x_i^k - \hat{x}_i^k\|^2 + \theta_i(x_i^k) \\ & \geq \langle x_i^{k+1} - \hat{x}_i^k, \nabla_i h(\hat{x}_i^k, x_{\neq i}^{k,i}) \rangle + \frac{1}{2\gamma_i^k} \|x_i^{k+1} - \hat{x}_i^k\|^2 + \theta_i(x_i^{k+1}). \end{aligned} \quad (16)$$

Hence,

$$\begin{aligned} & \langle x_i^k - x_i^{k+1}, \nabla_i h(\hat{x}_i^k, x_{\neq i}^{k,i}) \rangle + \frac{1}{2\gamma_i^k} \|x_i^k - \hat{x}_i^k\|^2 + \theta_i(x_i^k) \\ & \geq \frac{1}{2\gamma_i^k} \|x_i^{k+1} - \hat{x}_i^k\|^2 + \theta_i(x_i^{k+1}). \end{aligned} \quad (17)$$

Since  $\nabla_i h$  is Lipschitz continuous, we have

$$h(x_{<i}^{k+1}, x_i^{k+1}, x_{>i}^k) - h(x_{<i}^{k+1}, x_i^k, x_{>i}^k) - \langle x_i^{k+1} - x_i^k, \nabla_i h(x_{<i}^{k+1}, x_i^k, x_{>i}^k) \rangle \leq \frac{L_i^k}{2} \|x_i^{k+1} - x_i^k\|^2. \quad (18)$$

Combining (17) and (18), and recalling the definition of  $F$  in (3), we have

$$\begin{aligned} & F(x_{<i}^{k+1}, x_i^k, x_{>i}^k) + \langle x_i^{k+1} - x_i^k, \nabla_i h(x_{<i}^{k+1}, x_i^k, x_{>i}^k) - \nabla_i h(\hat{x}_i^k, x_{\neq i}^{k,i}) \rangle \\ & \geq F(x_{<i}^{k+1}, x_i^{k+1}, x_{>i}^k) + \frac{1}{2\gamma_i^k} \|x_i^{k+1} - \hat{x}_i^k\|^2 - \frac{1}{2\gamma_i^k} \|x_i^k - \hat{x}_i^k\|^2 - \frac{L_i^k}{2} \|x_i^{k+1} - x_i^k\|^2 \\ & = F(x_{<i}^{k+1}, x_i^{k+1}, x_{>i}^k) + \frac{1}{2\gamma_i^k} \|x_i^{k+1} - x_i^k\|^2 - \frac{\alpha_i^k}{\gamma_i^k} \langle x_i^{k+1} - x_i^k, x_i^k - x_i^{k-1} \rangle - \frac{L_i^k}{2} \|x_i^{k+1} - x_i^k\|^2 \\ & \geq F(x_{<i}^{k+1}, x_i^{k+1}, x_{>i}^k) + \frac{1 - \alpha_i^k - \gamma_i^k L_i^k}{2\gamma_i^k} \|x_i^{k+1} - x_i^k\|^2 - \frac{\alpha_i^k}{2\gamma_i^k} \|x_i^k - x_i^{k-1}\|^2, \end{aligned} \quad (19)$$

Note that

$$\begin{aligned} & \langle x_i^{k+1} - x_i^k, \nabla_i h(x_{<i}^{k+1}, x_i^k, x_{>i}^k) - \nabla_i h(\hat{x}_i^k, x_{\neq i}^{k,i}) \rangle \\ & = \langle x_i^{k+1} - x_i^k, \nabla_i h(x_{<i}^{k+1}, x_i^k, x_{>i}^k) - \nabla_i h(x^{k,i}) \rangle + \langle x_i^{k+1} - x_i^k, \nabla_i h(x^{k,i}) - \nabla_i h(\hat{x}_i^k, x_{\neq i}^{k,i}) \rangle \\ & \leq \|x_i^{k+1} - x_i^k\| \|\nabla_i h(x_{<i}^{k+1}, x_i^k, x_{>i}^k) - \nabla_i h(x^{k,i})\| + \frac{\alpha_i^k L_i^k}{2} \|x_i^{k+1} - x_i^k\|^2 + \frac{\alpha_i^k L_i^k}{2} \|x_i^k - x_i^{k-1}\|^2 \\ & \leq \|x_i^{k+1} - x_i^k\| \left( \sum_{j=1}^{i-1} w_{ij} L^k \|x_j^{k+1} - x_j^k\| \right) + \frac{\alpha_i^k L_i^k}{2} \|x_i^{k+1} - x_i^k\|^2 + \frac{\alpha_i^k L_i^k}{2} \|x_i^k - x_i^{k-1}\|^2, \end{aligned} \quad (20)$$

where  $L^k = \max_i \{L_i^k, i = 1, 2, \dots, p\}$ . Since  $F(x^{k+1}) - F(x^k) = \sum_{i=1}^p (F(x_{<i}^{k+1}, x_i^{k+1}, x_{>i}^k) - F(x_{<i}^{k+1}, x_i^k, x_{>i}^k))$  with  $x^{k+1} = \{x_i^{k+1}, \dots, x_p^{k+1}\}$  and  $x^k = \{x_i^k, \dots, x_p^k\}$  according to the definition of  $F$  in (3), it follows from (19) and (20) that

$$\begin{aligned} & F(x^k) + \sum_{i=1}^p \frac{\alpha_i^k \gamma_i^k L_i^k + \alpha_i^k}{2\gamma_i^k} \|x_i^k - x_i^{k-1}\|^2 \\ & \geq F(x^{k+1}) + \sum_{i=1}^p \frac{1 - \alpha_i^k - \gamma_i^k L_i^k - \alpha_i^k \gamma_i^k L_i^k}{2\gamma_i^k} \|x_i^{k+1} - x_i^k\|^2 \\ & \quad - \sum_{i=1}^p \|x_i^{k+1} - x_i^k\| \left( \sum_{j=1}^{i-1} w_{ij} L^k \|x_j^{k+1} - x_j^k\| \right) \\ & \geq F(x^{k+1}) + \sum_{i=1}^p \frac{1 - \alpha_i^k - \gamma_i^k L_i^k - \alpha_i^k \gamma_i^k L_i^k}{2\gamma_i^k} \|x_i^{k+1} - x_i^k\|^2 - \frac{w'_i L^k}{2} \sum_{i=1}^p \|x_i^{k+1} - x_i^k\|^2 \\ & = F(x^{k+1}) + \sum_{i=1}^p \frac{1 - \alpha_i^k - \gamma_i^k L_i^k - \alpha_i^k \gamma_i^k L_i^k - \gamma_i^k w'_i L^k}{2\gamma_i^k} \|x_i^{k+1} - x_i^k\|^2, \end{aligned} \quad (21)$$

where  $w'_i = \sum_{q=i+1}^p w_{qi}$ . This completes the proof.  $\square$

## C Proof of Lemma 1

*Proof.* (i) It follows from Proposition 1 that

$$F(x^k) + \sum_{i=1}^p \frac{\xi_i^k}{2} \|x_i^k - x_i^{k-1}\|^2 \geq F(x^{k+1}) + \sum_{i=1}^p \frac{\delta_i^k}{2} \|x_i^{k+1} - x_i^k\|^2, k = 1, 2, \dots, \quad (22)$$

where  $\xi_i^k$  and  $\delta_i^k$  are positive parameters and  $\xi_i^{k+1} \leq C \delta_i^k$  for some constant  $C \in (0, 1)$ . Hence, we have

$$F(x^{k+1}) + \sum_{i=1}^p \frac{\delta_i^k}{2} \|x_i^{k+1} - x_i^k\|^2 \leq F(x^k) + \sum_{i=1}^p C \frac{\delta_i^{k-1}}{2} \|x_i^k - x_i^{k-1}\|^2. \quad (23)$$



Summing up  $k = 0$  to  $K - 1$ , we get

$$\begin{aligned} F(x^K) &+ \sum_{i=1}^p \frac{\delta_i^{K-1}}{2} \|x_i^K - x_i^{K-1}\|^2 + (1-C) \sum_{k=0}^{K-1} \sum_{i=1}^p \frac{\delta_i^k}{2} \|x_i^{k+1} - x_i^k\|^2 \\ &\leq F(x^0) + \sum_{i=1}^p C \frac{\delta_i^{-1}}{2} \|x_i^0 - x_i^{-1}\|^2. \end{aligned} \quad (24)$$

This completes the proof.  $\square$

## D Proof of Theorem 1

*Proof.* Suppose a subsequence  $\{x^{k_n}\}$  of  $\{x^k\}$  converges to  $x^* \in \mathcal{X}$ . Lemma 1 implies that  $x^{k_n-1} \rightarrow x^*$  and  $x^{k_n+1} \rightarrow x^*$ . Choosing  $x_i = x_i^*$  and  $k = k_n$  in (16), we obtain

$$\begin{aligned} &\langle x_i^* - x_i^{k_n+1}, \nabla_i h(\hat{x}_i^{k_n}, x_{\neq i}^{k_n}) \rangle + \frac{1}{2\gamma_i^{k_n}} \|x_i^* - \hat{x}_i^{k_n}\|^2 + \theta_i(x_i^*) \\ &\geq \frac{1}{2\gamma_i^{k_n}} \|x_i^{k_n+1} - \hat{x}_i^{k_n}\|^2 + \theta_i(x_i^{k_n+1}). \end{aligned} \quad (25)$$

Since  $\nabla_i h$  is Lipschitz continuous, we have

$$h(x_{<i}^{k_n+1}, x_i^{k_n+1}, x_{>i}^{k_n}) - h(x_{<i}^{k_n+1}, x_i^*, x_{>i}^{k_n}) - \langle x_i^{k_n+1} - x_i^*, \nabla_i h(x_{<i}^{k_n+1}, x_i^*, x_{>i}^{k_n}) \rangle \leq \frac{L_i^{k_n}}{2} \|x_i^{k_n+1} - x_i^*\|^2. \quad (26)$$

From the definition of  $F$ , we have

$$\limsup_{n \rightarrow \infty} \frac{1}{2\gamma_i^{k_n}} \|x_i^{k_n+1} - \hat{x}_i^{k_n}\|^2 + h(x_{<i}^{k_n+1}, x_i^{k_n+1}, x_{>i}^{k_n}) + \theta_i(x_i^{k_n+1}) \leq F(x^*). \quad (27)$$

From the low semi-continuous and for  $x_i$ , we have

$$F(x^*) \leq h(x_{<i}^*, x_i, x_{>i}^*) + \theta_i(x_i), \quad (28)$$

which means that  $x_i^*$  is the minimiser of the problem

$$\min_{x_i} h(x_{<i}^*, x_i, x_{>i}^*) + \theta_i(x_i). \quad (29)$$

Then from the optimality condition, we complete the proof.  $\square$

## E Proof of Theorem 2

**Assumption 2.** ([20], assumption 3) Let  $u_i(x, z) = h(z) + \frac{1}{2\gamma_i^k} \|x - z\|^2 + \langle x - z, \nabla_i h(z) \rangle$ , for any bounded subset of  $\mathcal{X}$  and any  $x, z$  in this subset, for  $s_i \in \partial_{x_i} u_i(x, z)$ , there exists  $t_i \in \partial_{x_i} f(x)$  such that

$$\|s_i - t_i\| \leq B_i \|x - z\|$$

for some constant  $B_i$  that may depend on the subset.

**Lemma 2.** ([26], Theorem 2) Let  $\Phi : \mathbb{R}^N \rightarrow (-\infty, +\infty]$  be a proper and lower semicontinuous function which is bounded from below. Let  $\mathcal{A}$  be a generic algorithm which generates a bounded sequence  $\{z^k\}$  by  $z^0 \in \mathbb{R}^N, z^{k+1} \in \mathcal{A}(z^k), k = 0, 1, \dots$ . Assume that there exist positive constants  $\rho_1, \rho_2$  and  $\rho_3$  and a non-negative sequence  $\{\varphi_k\}_{k \in \mathbb{N}}$  such that the following conditions are satisfied:

(i) Sufficient decrease property:

$$\rho_1 \|z^k - z^{k+1}\|^2 \leq \rho_2 \varphi_k^2 \leq \Phi(z^k) - \Phi(z^{k+1}), k = 0, 1, \dots$$

(ii) Boundedness of subgradient:

$$\|\omega^{k+1}\| \leq \rho_3 \varphi_k, \omega^k \in \partial \Phi(z^k) \text{ for } k = 0, 1, \dots$$

(iii) *KL property*:  $\Phi$  is a KL function.

(iv) *A continuity condition*: If a subsequence  $\{z^{k_n}\}$  converges to  $\bar{z}$  then  $\Phi(z^{k_n})$  converges to  $\Phi(\bar{z})$  as  $n$  goes to  $\infty$ .

Then we have  $\sum_{k=1}^{\infty} \varphi_k < \infty$ , and  $\{z^k\}$  converges to a critical point of  $\Phi$ .

Hence, according to the Assumption 2 and Lemma 2, we prove theorem 2 as follows.

*Proof.* Let  $x^*$  be a limit point of  $x^k$ . From Theorem 1 we have  $x^*$  is a critical point. Define  $F^\delta(x, y) := F(x) + \sum_{i=1}^m \frac{\delta_i}{2} \|x_i - y_i\|^2$ . Let  $z^k = (x^k, x^{k-1})$ ,  $\varphi_k^2 = \frac{1}{2} \|x^{k+1} - x^k\|^2 + \frac{1}{2} \|x^k - x^{k-1}\|^2$ . As the generated sequence  $\{x^k\}$  is assumed to be bounded in the following, we verify the conditions of Lemma 2 for  $F^\delta(x^k, x^{k-1})$  with  $\delta_i = (\underline{l} + C\bar{l})/2$ .

(i) *Sufficient decrease property*:

From (23), we have

$$F(x^{k+1}) + \underline{l} \|x_i^{k+1} - x_i^k\|^2 \leq F(x^k) + C\bar{l} \|x_i^k - x_i^{k-1}\|^2, \quad (30)$$

hence,  $F^\delta(z^k) - F^\delta(z^{k+1}) \geq (\underline{l} - C\bar{l})\varphi_k^2$ .

(ii) *Boundedness of subgradient*:

Note that  $\partial_x F^\delta(x, y) = \partial F(x) + [\delta_i(x_i - y_i)|_{i=1, \dots, m}]$  and  $\partial_y F^\delta(x, y) = [\delta_i(y_i - x_i)|_{i=1, \dots, m}]$ , with the optimality condition we have

$$\nabla_i h(x_i^k, \bar{x}_{\neq i}^{k+1}) - \nabla_i h(\bar{x}^{k+1, i}) + \frac{\alpha_i^k}{\gamma_i^k} (x_i^k - x_i^{k-1}) \in \partial_{x_i} (u_i(\bar{x}_i^{k+1}, \bar{x}_{\neq i}^{k+1}) + \theta_i(\bar{x}_i^{k+1})). \quad (31)$$

By Assumption 2, there exist  $s_i^k \in \partial_{x_i} u_i(\bar{x}_i^{k+1}, \bar{x}_{\neq i}^{k+1})$  and  $v_i^k \in \partial \theta_i(\bar{x}_i^{k+1})$  such that

$$\nabla_i h(x_i^k, \bar{x}_{\neq i}^{k+1}) - \nabla_i h(\bar{x}^{k+1, i}) + \frac{\alpha_i^k}{\gamma_i^k} (x_i^k - x_i^{k-1}) = s_i^k + v_i^k, \quad (32)$$

and there exists  $t_i^k \in \partial_{x_i} h(x^{k+1})$  such that

$$\|s_i^k - t_i^k\| \leq B_i \|x^{k+1} - (x_i^k, \bar{x}_{\neq i}^{k+1})\|. \quad (33)$$

We note that  $t_i^k + v_i^k \in \partial_{x_i} F(x^{k+1})$  by Assumption 2. On the other hand,

$$\|t_i^k + v_i^k\| = \|t_i^k - s_i^k + s_i^k + v_i^k\| \leq B_i \|x^{k+1} - (x_i^k, \bar{x}_{\neq i}^{k+1})\| + \frac{2\alpha_i^k}{\gamma_i^k} \|x_i^k - x_i^{k-1}\|, \quad (34)$$

which implies the boundedness of the subgradient.

(iii) *KL property*:

Since  $F$  is a KL function,  $F^\delta$  is also a KL function.

(iv) *A continuity condition*:

Suppose  $z^{k_n} \rightarrow z^*$ , Lemma 1 implies that if  $x^{k_n} \rightarrow x^*$ , then  $x^{k_n-1} \rightarrow x^*$ . Hence  $z^* = (x^*, x^*)$ . On the other hand, we know that for  $i \in [p]$ ,  $h(x_i^{k_n}, \bar{x}_{\neq i}^{k_n-1}) + \theta_i(x_i^{k_n}) \rightarrow h(x^*) + \theta_i(x_i^*)$ . Hence  $F(x^{k_n})$  converges to  $F(x^*)$ , which leads to  $F^\delta(z^{k_n+1})$  converges to  $F^\delta(z^*)$ .

From Lemma 2, the whole generated sequence  $\{x^k\}$  of the proposed iBPLM algorithm is convergent.  $\square$

## F Additional Results

In this section, we report the parameter analysis and comprehensive experimental results of our proposed iBPLM and PnP-iBPLM methods.

First of all, we plot the PSNR, SSIM, and energy curves of our methods in Figure 3 to showcase the performance of different weight parameter  $\tau_X$  values from iteration 2 to 8. The extrapolated parameters  $\alpha_X$  and  $\alpha_D$  are analyzed in Figure 4. Specifically, the range of  $\alpha_X$  and  $\alpha_D$  is set to  $[0.001, 0.25, 0.5, 0.75, 0.999]$ . The PSNR surface indicates that the final performance is influenced by the extrapolated parameters. Furthermore, we plot the energy curves of inertial parameter  $\alpha_X$  (with  $\alpha_D = 0.5$  fixed) and  $\alpha_D$  (with  $\alpha_X = 0.5$  fixed) along the iteration. Specifically, variations in  $\alpha_X$  and  $\alpha_D$  lead to different energy convergence rates, showcasing the importance of these parameters in refining the model’s efficiency and effectiveness. Overall, these results underscore the robustness of our proposed denoising model and the beneficial role of parameter tuning in achieving superior image quality.

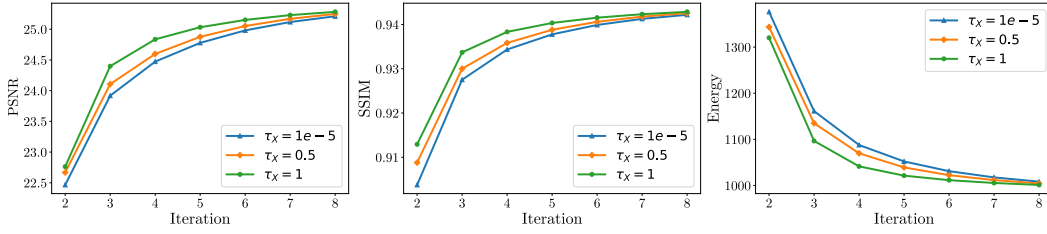


Figure 3: PSNR, SSIM, and energy curves of the proposed methods with different  $\tau_X$  values from iteration 2 to 8.

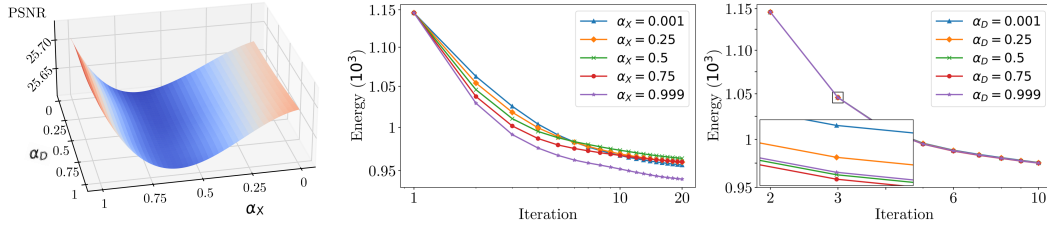


Figure 4: Effect of  $\alpha_X$  and  $\alpha_D$  in iBPLM algorithm on ‘butterfly’ with noise level 25. The first image is the PSNR surface under different  $\alpha_X$  and  $\alpha_D$ . The second one is the energy curves of different  $\alpha_X$  with fixed  $\alpha_D = 0.5$ . The third one is the energy curves of different  $\alpha_D$  with fixed  $\alpha_X = 0.5$ . The comparisons of the second and third plots are conducted through log-log scale analysis.

Secondly, we give the detailed settings of the dictionary learning image restoration model. For better understanding, we rewrite a more comprehensive solution of our proposed PnP-iBPLM scheme for dictionary learning. Given the input image  $Y$  with some linear operator  $B$ , the image restoration model can be formulated as

$$\min_{X, D, I, Z} \frac{\eta}{2} \|DX - I\|^2 + \frac{\beta}{2} \|I - Z\|^2 + \lambda_X \phi_X(X) + \lambda_D \phi_D(D) + \lambda_Z \phi_Z(Z) + \frac{\lambda_I}{2} \|BI - Y\|^2, \quad (35)$$

where  $D$  is the dictionary,  $X$  is the corresponding sparse coefficient,  $I$  is the latent image,  $\eta$ ,  $\beta$ ,  $\lambda_X$ ,  $\lambda_D$ ,  $\lambda_Z$ , and  $\lambda_I$  are positive parameters. The  $\phi_D$ ,  $\phi_X$ , and  $\phi_Z$  terms are the regularizers for  $D$ ,  $X$ ,  $Z$ , respectively. Following the proposed PnP-iBPLM algorithm, this model can be solved by letting  $h(X, D, I, Z) = \frac{\eta}{2} \|DX - I\|^2 + \frac{\beta}{2} \|I - Z\|^2$ ,  $\theta_X(X) = \lambda_X \phi_X(X)$ ,  $\theta_D(D) = \lambda_D \phi_D(D)$ ,  $\theta_I(I) = \frac{\lambda_I}{2} \|BI - Y\|^2$ ,  $\theta_Z(Z) = \lambda_Z \phi_Z(Z)$  with regularizers are gradient step denoisers. However, we simplify the iteration by applying only one denoiser in  $\theta_Z$ . For the variables  $D$  and  $X$  in the dictionary learning method, we use the regularizer according to their definition to better fit the meaning of the model. For  $\theta_I$ , we use the data-fitting term to constrain the image restoration model. The following are the more specific settings.

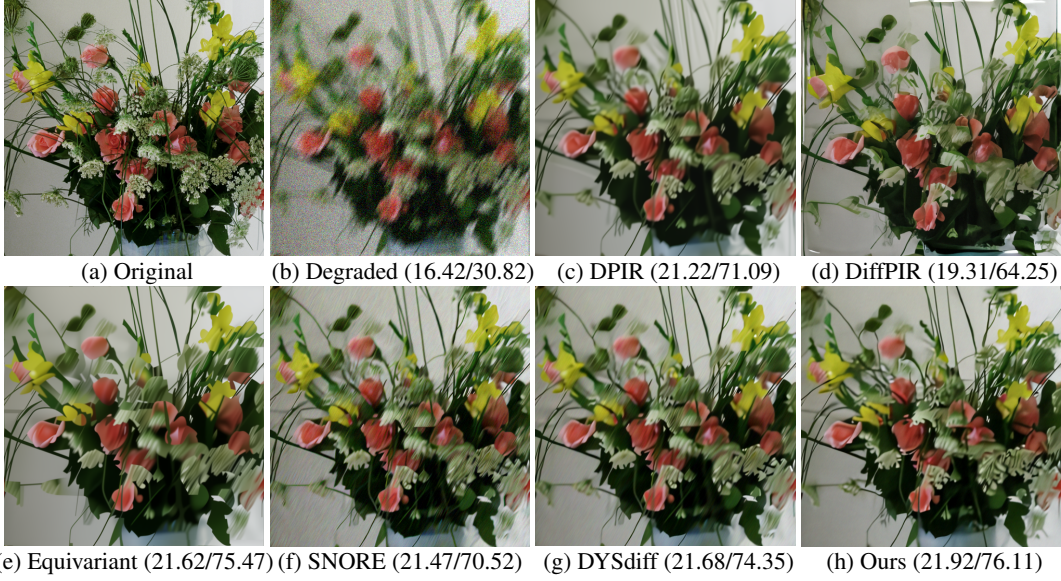


Figure 5: Image restoration results (PSNR/SSIM) with motion blur kernel MB(20, 60) and Gaussian noise level 25. Visualisation comparison of our scheme and some state-of-the-art PnP-based methods: (c) DPIP [64], (d) DiffPIR [66], (e) Equivariant [48], (f) SNORE [39], (g) DYSDiff [55], and (h) Our PnP-iBPLM.

For  $X$ -subproblem, we have

$$X^{k+1} \in \arg \min_X \frac{1}{2\gamma_X} \left\| X - \hat{X}^k + \gamma_X \hat{h}_X^k \right\|^2 + \lambda_X \phi_X(X), \quad (36)$$

where  $\hat{h}_X^k = \eta D^{kT} (D^k \hat{X}^k - I^k)$ ,  $\hat{X}^k = X^k + \alpha_X (X^k - X^{k-1})$ ,  $D^{kT}$  is the conjugate of  $D^k$ ,  $\alpha_D \in [0, 1]$ , and  $\gamma_X \in (0, 1/L_X)$ ,  $L_X$  is the Lipschitz constant. Following the definition of the traditional dictionary learning model, we set  $\phi_X(X) = \|X\|_0$  to describe the sparsity of the coefficients. Hence, the  $X$ -subproblem can be solved by the hard-shrinkage method.

For  $D$ -subproblem, we have

$$D^{k+1} \in \arg \min_D \frac{1}{2\gamma_D} \left\| D - \hat{D}^k + \gamma_D \hat{h}_D^k \right\|^2 + \lambda_D \phi_D(D), \quad (37)$$

where  $\hat{h}_D^k = \eta (\hat{D}^k \bar{X}^k - I^k) \bar{X}^{kT}$ ,  $\hat{D}^k = D^k + \alpha_D (D^k - D^{k-1})$ ,  $\bar{X}^k = X^k + \tau_X (X^{k+1} - X^k)$ ,  $\bar{X}^{kT}$  is the conjugate of  $\bar{X}^k$ ,  $\alpha_D \in [0, 1]$ ,  $\tau_X \in [0, 1]$ , and  $\gamma_D \in (0, 1/L_D)$ ,  $L_D$  is the Lipschitz constant. Following the definition of the traditional dictionary learning model, we set  $\phi_D(D) = \|D\|^2$ . Hence, the  $D$ -subproblem has a close-formed solution.

For  $I$ -subproblem, we get

$$I^{k+1} = \arg \min_I \frac{1}{2\gamma_I} \left\| I - \hat{I}^k + \gamma_I \hat{h}_I^k \right\|^2 + \frac{\lambda_I}{2} \|BI - Y\|^2, \quad (38)$$

with  $\hat{h}_I^k = \eta (\hat{I}^k - \bar{D}^k \bar{X}^k) + \gamma (\hat{I}^k - Z^k)$ ,  $\hat{I}^k = I^k + \alpha_I (I^k - I^{k-1})$ ,  $\bar{D}^k = D^k + \tau_D (D^{k+1} - D^k)$ ,  $\bar{X}^k = X^k + \tau_X (X^{k+1} - X^k)$ ,  $\alpha_I \in [0, 1]$ ,  $\tau_D \in [0, 1]$ ,  $\tau_X \in [0, 1]$ , and  $\gamma_I \in (0, 1/L_I)$ ,  $L_I$  is the Lipschitz constant.  $I$ -subproblem also has a close-formed solution.

For the  $Z$ -subproblem

$$Z^{k+1} \in \arg \min_Z \frac{1}{2\gamma_Z} \left\| Z - \hat{Z}^k + \gamma_Z \hat{h}_Z^k \right\|^2 + \lambda_Z \phi_Z(Z), \quad (39)$$

where  $\hat{h}_Z^k = \beta (\hat{Z}^k - \bar{I}^k)$ ,  $\hat{Z}^k = Z^k + \alpha_Z (Z^k - Z^{k-1})$ ,  $\bar{I}^k = I^k + \tau_I (I^{k+1} - I^k)$ ,  $\tau_I \in [0, 1]$ , and  $\gamma_Z \in (0, 1/L_Z)$ ,  $L_Z$  is the Lipschitz constant. Hence it can be solved by a deep denoiser

$$Z^{k+1} = \mathcal{D}_\sigma \left( \hat{Z}^k - \gamma_Z \hat{h}_Z^k, \sqrt{\gamma_Z \lambda_Z} \right). \quad (40)$$

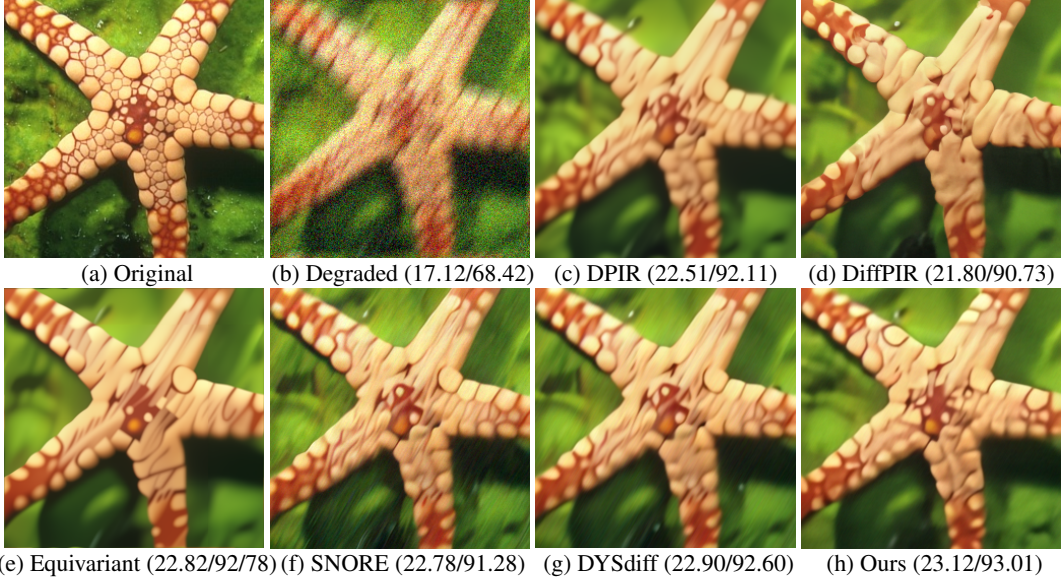


Figure 6: Image restoration results (PSNR/SSIM) with motion blur kernel MB(20, 60) and Gaussian noise level 25. Visualisation comparison of our scheme and some state-of-the-art PnP-based methods: (c) DPIR [64], (d) DiffPIR [66], (e) Equivariant [48], (f) SNORE [39], (g) DYSDiff [55], and (h) Our PnP-iBPLM.

More specifically, we use the classical DRUNet [64] as our deep gradient step denoiser. DRUNet incorporates both U-Net and ResNet architectures and takes an additional noise level map as input, achieving state-of-the-art performance in Gaussian noise removal. Similar to the setting in [55; 24], we regularize the training loss of  $\mathcal{D}_\sigma$  using the spectral norm  $\|\cdot\|_S$  of the Hessian of  $g_\sigma$  as follows

$$\mathcal{L}_S(\sigma) = \mathbb{E}_{\mathbf{x} \sim p, \xi_\sigma \sim \mathcal{N}(0, \sigma^2)} \left[ \|\mathcal{D}_\sigma(\mathbf{x} + \xi_\sigma) - \mathbf{x}\|^2 + 0.01 \max(\|\nabla^2 g_\sigma(\mathbf{x} + \xi_\sigma)\|_S, 0.9) \right] \quad (41)$$

to ensure the Lipschitz constant of  $\nabla g_\sigma$  is less than 1, which is consistent with Section 3.2. Berkeley segmentation dataset, Waterloo Exploration Database, DIV2K dataset, and Flick2K dataset are applied as the training sets.

Note that we follow the setting in the [55; 24], only noise level  $\{2.55, 7.65, 12.75\}$  are considered in training. After training, we apply the pre-trained deep gradient step neural network as the denoiser to handle the image restoration problem of heavy Gaussian noise. Experiments show that our method can even handle the image corrupted with heavy motion blur and Gaussian noise.

The evaluations are based on standard metrics, such as the Peak Signal-to-Noise Ratio (PSNR) and Structural Similarity Index (SSIM), applied to multiple classical datasets. Our experiments demonstrate the robustness and superiority of our algorithms compared to existing methods.

We conducted extensive tests to compare the performance of PnP-iBPLM with other state-of-the-art image restoration algorithms. Figures 5 and 6 illustrate the visual results for different images, including motion blur and Gaussian noise. The metrics (PSNR/SSIM) for these tests indicate that our method consistently yields higher values, signifying better restoration quality.

Tables 4, 5, and 6 present the PSNR and SSIM values for different image restoration models evaluated on the Set3C, Set17, Kodak24, CBSD10, and Set18 datasets, with a motion blur kernel MB(20,60) and Gaussian noise level 25. The tables list the performance of each model for individual images and include an average score for both datasets. From the average results, it is clear that our proposed method, PnP-iBPLM, consistently achieves the highest scores.

Table 4: PSNR (dB) and SSIM (%) results of different restoration models for MB(20, 60)/ $\sigma = 25$ . We refer to 'Equivariant' as 'Equi.', and denote our approach with a ★.

	Index	Degraded	DPIR [64]	DiffPIR [66]	Equi. [48]	SNORE [39]	DYSDiff [55]	★PnP-iBPLM
Set3C								
butterfly	PSNR	13.93	20.11	20.91	23.01	22.47	23.00	23.31
	SSIM	56.99	85.32	87.66	91.29	89.71	91.01	92.06
leaves	PSNR	13.21	19.52	19.23	22.63	21.16	22.13	22.72
	SSIM	27.12	76.58	77.83	87.99	79.85	84.76	87.06
starfish	PSNR	17.12	22.51	21.80	22.82	22.78	22.90	23.12
	SSIM	68.42	92.11	90.73	92.78	91.28	92.60	93.01
Ave.	PSNR	14.75	20.78	20.64	22.82	22.14	22.67	23.05
	SSIM	50.85	84.67	85.41	90.68	86.95	89.46	90.71
Set17								
img0	PSNR	16.27	22.21	19.14	18.90	22.74	22.70	22.91
	SSIM	58.74	59.85	79.28	59.60	88.62	88.91	89.42
img10	PSNR	17.07	23.08	22.34	27.97	25.26	25.47	26.12
	SSIM	59.30	89.71	72.70	90.62	87.16	91.06	92.19
img11	PSNR	19.62	27.67	27.05	23.20	28.48	29.24	29.58
	SSIM	46.56	71.94	83.11	75.41	89.73	92.79	93.60
img12	PSNR	15.55	18.98	17.24	25.88	19.08	19.19	19.40
	SSIM	33.65	74.21	52.05	94.39	60.79	62.06	63.29
img13	PSNR	19.67	26.85	24.77	28.36	27.26	27.78	27.84
	SSIM	85.62	97.03	95.94	98.39	97.67	98.07	98.17
img14	PSNR	17.70	26.17	25.51	27.27	26.40	26.75	27.10
	SSIM	52.98	90.78	89.92	92.04	90.62	91.70	92.12
img15	PSNR	18.14	23.52	23.44	24.68	24.25	24.61	24.93
	SSIM	36.31	82.14	80.65	83.63	78.43	82.75	83.81
img16	PSNR	18.96	26.54	25.20	26.23	25.87	26.42	26.64
	SSIM	30.56	77.80	73.02	76.92	73.80	77.46	78.08
img1	PSNR	17.52	22.58	21.74	23.44	22.40	22.64	22.93
	SSIM	29.12	85.74	64.21	90.57	66.40	68.79	70.36
img2	PSNR	18.33	24.84	23.92	21.86	24.23	24.67	25.02
	SSIM	22.24	77.19	68.10	77.57	66.08	71.44	73.31
img3	PSNR	17.49	23.49	22.59	22.66	23.67	23.82	24.28
	SSIM	23.36	68.26	74.89	69.07	69.12	76.62	79.54
img4	PSNR	17.44	21.79	21.15	30.42	22.04	21.89	21.92
	SSIM	46.18	84.44	64.81	94.71	74.31	68.36	68.25
img5	PSNR	17.29	21.87	19.34	24.64	21.77	22.12	22.35
	SSIM	37.40	72.48	65.44	72.52	68.14	77.64	78.86
img6	PSNR	17.33	22.10	20.79	24.03	21.98	22.21	22.30
	SSIM	29.86	78.33	57.01	80.53	63.77	65.32	66.03
img7	PSNR	18.95	25.58	25.01	21.96	25.25	25.73	25.84
	SSIM	43.44	67.28	79.08	67.90	78.70	81.21	81.60
img8	PSNR	18.48	26.96	25.83	21.74	27.28	27.35	28.00
	SSIM	57.79	63.74	87.72	62.40	87.15	89.35	90.27
img9	PSNR	16.57	22.54	21.85	25.73	22.97	23.27	23.32
	SSIM	24.23	80.78	67.72	80.98	69.92	74.36	75.46
Ave.	PSNR	17.79	24.16	22.76	24.65	24.17	24.46	24.74
	SSIM	42.20	77.75	73.86	80.42	77.08	79.88	80.85

Table 5: PSNR (dB) and SSIM (%) results of different restoration models for MB(20, 60)/ $\sigma = 25$ . We refer to 'Equivariant' as 'Equi.', and denote our approach with a ★.

	Index	Degraded	DPIR [64]	DiffPIR [66]	Equi. [48]	SNORE [39]	DYSdiff [55]	★PnP-iBPLM
Kodoak24								
img0	PSNR	17.18	21.80	21.33	21.99	21.83	22.03	22.39
	SSIM	32.24	63.49	60.98	64.85	63.32	64.57	66.51
img10	PSNR	18.38	24.53	23.85	24.84	24.39	24.70	24.96
	SSIM	29.05	78.89	76.53	81.08	73.28	78.23	79.69
img11	PSNR	18.94	27.58	27.19	27.76	27.23	28.08	28.62
	SSIM	41.80	90.21	89.19	90.99	86.66	90.07	90.98
img12	PSNR	16.46	20.01	19.32	19.94	19.96	20.11	20.22
	SSIM	33.26	63.34	59.96	63.79	62.91	64.49	65.07
img13	PSNR	17.93	23.46	22.58	23.60	23.29	23.64	23.75
	SSIM	33.68	70.64	67.51	71.58	67.14	70.98	71.55
img14	PSNR	19.14	26.89	26.65	28.36	27.05	27.87	28.16
	SSIM	42.22	88.64	87.60	91.24	85.20	89.49	90.30
img15	PSNR	19.14	26.58	26.09	26.72	25.85	26.53	26.70
	SSIM	22.94	72.04	70.01	72.46	64.52	70.66	71.89
img16	PSNR	19.07	26.43	25.31	26.95	25.95	26.56	26.81
	SSIM	21.87	80.05	75.41	82.62	70.74	79.03	80.63
img17	PSNR	18.08	23.31	22.68	23.49	23.23	23.38	23.67
	SSIM	34.74	75.83	72.73	77.39	71.10	75.53	76.49
img18	PSNR	17.83	23.98	23.23	24.31	23.92	24.25	24.50
	SSIM	32.27	83.69	81.21	84.54	76.45	82.54	83.98
img19	PSNR	18.92	25.20	24.99	27.02	26.51	26.78	27.35
	SSIM	36.61	86.85	84.80	89.99	83.02	87.98	89.34
img1	PSNR	19.47	27.73	27.27	27.78	27.03	27.68	28.09
	SSIM	83.42	96.89	96.57	96.91	96.38	96.88	97.17
img20	PSNR	17.87	23.61	22.82	23.58	23.40	23.63	24.02
	SSIM	35.38	77.48	74.35	77.34	73.84	76.90	78.50
img21	PSNR	18.57	25.36	24.92	25.43	25.18	25.72	25.86
	SSIM	40.48	84.30	82.68	84.42	79.56	84.08	84.83
img22	PSNR	19.18	28.02	26.95	28.70	27.26	28.18	29.06
	SSIM	52.78	94.59	93.12	95.17	89.88	93.78	94.75
img23	PSNR	17.38	22.39	22.07	22.90	22.56	22.84	23.01
	SSIM	24.70	71.11	68.22	73.44	67.20	71.87	72.99
img2	PSNR	19.29	28.36	27.83	29.08	27.71	28.60	28.91
	SSIM	42.50	93.10	92.02	94.03	86.32	91.77	92.93
img3	PSNR	19.06	27.53	26.82	27.49	27.03	27.54	27.80
	SSIM	56.74	94.31	93.25	94.45	91.86	93.82	94.38
img4	PSNR	16.44	21.07	20.43	21.61	21.28	21.50	21.68
	SSIM	30.13	65.61	61.57	68.98	65.62	67.68	68.85
img5	PSNR	17.99	23.15	22.64	23.10	23.01	23.27	23.52
	SSIM	36.43	73.28	71.34	73.15	70.84	73.12	74.33
img6	PSNR	18.39	25.77	24.61	25.53	25.48	25.84	26.17
	SSIM	37.27	87.43	83.86	86.30	82.98	86.24	87.67
img7	PSNR	15.55	20.13	19.74	21.00	20.57	20.77	21.21
	SSIM	26.63	64.02	61.05	68.58	64.49	66.19	68.87
img8	PSNR	18.67	27.02	26.02	27.88	26.46	26.99	27.72
	SSIM	20.98	81.31	77.89	82.60	70.30	78.54	81.06
img9	PSNR	18.94	27.35	26.17	27.04	26.66	27.42	27.85
	SSIM	23.09	82.18	78.39	82.62	73.88	80.45	81.93
Ave.	PSNR	18.24	24.99	24.23	25.25	24.70	25.16	25.50
	SSIM	36.30	79.97	77.51	81.19	75.73	79.79	81.03

Table 6: PSNR (dB) and SSIM (%) results of different restoration models for MB(20, 60)/ $\sigma = 25$ . We refer to 'Equivariant' as 'Equi.', and denote our approach with a  $\star$ .

	Index	Degraded	DPIR [64]	DiffPIR [66]	Equi. [48]	SNORE [39]	DYSdiff [55]	$\star$ PnP-iBPLM
CBSD10								
img0	PSNR	19.50	32.28	31.53	35.06	30.64	32.79	33.71
	SSIM	20.49	95.72	93.96	96.87	81.74	92.54	94.74
img1	PSNR	17.83	23.13	22.09	23.00	22.96	23.09	23.23
	SSIM	52.30	81.32	77.69	80.90	80.84	81.46	81.86
img2	PSNR	19.66	28.79	28.09	29.98	28.37	29.47	29.74
	SSIM	43.15	87.35	85.29	90.41	82.50	88.13	89.23
img3	PSNR	18.12	23.92	23.15	24.03	23.75	24.04	24.13
	SSIM	37.47	77.94	75.03	78.34	74.33	77.78	78.43
img4	PSNR	17.53	23.25	22.44	23.29	23.21	23.36	23.60
	SSIM	27.93	68.67	65.22	68.79	65.35	68.67	69.68
img5	PSNR	17.00	22.85	22.59	23.88	23.49	23.77	24.07
	SSIM	20.20	63.97	62.12	67.66	62.39	66.32	68.05
img6	PSNR	16.01	21.69	21.02	23.14	22.86	23.19	23.46
	SSIM	22.86	74.58	70.90	79.99	72.80	77.98	79.95
img7	PSNR	14.50	17.93	17.13	17.73	18.02	18.11	18.31
	SSIM	27.77	54.29	47.96	52.73	55.21	55.63	57.65
img8	PSNR	17.03	21.18	20.59	21.29	21.24	21.36	21.47
	SSIM	25.58	54.14	50.61	54.89	54.99	56.07	56.51
img9	PSNR	18.62	24.73	23.79	26.00	25.56	25.96	25.94
	SSIM	33.07	84.71	80.95	86.36	78.97	84.77	85.58
Ave.	PSNR	17.58	24.14	23.24	24.74	24.01	24.51	24.77
	SSIM	31.08	74.27	70.97	75.70	70.91	74.94	76.17
Set18								
img0	PSNR	16.33	21.60	19.79	22.83	22.37	22.47	22.56
	SSIM	61.58	84.70	79.86	87.63	86.47	86.94	87.08
img10	PSNR	19.88	27.30	24.83	28.67	27.68	28.36	28.48
	SSIM	63.62	89.27	86.43	92.94	90.27	92.09	92.44
img11	PSNR	19.00	26.87	24.59	27.07	26.50	27.12	27.33
	SSIM	75.81	96.07	94.14	96.43	95.54	96.34	96.54
img12	PSNR	19.37	30.56	28.92	30.58	29.26	30.42	30.96
	SSIM	72.53	97.66	96.90	97.56	96.65	97.51	97.80
img13	PSNR	19.48	28.45	25.07	29.97	28.49	29.47	29.83
	SSIM	55.69	92.30	88.46	95.16	90.42	93.76	94.49
img14	PSNR	19.99	28.83	24.75	30.81	28.98	29.87	30.09
	SSIM	67.19	92.69	89.29	96.35	93.29	95.22	95.65
img15	PSNR	17.74	22.55	20.60	22.93	22.80	22.87	23.10
	SSIM	61.20	83.62	79.35	85.95	84.75	85.64	86.35
img16	PSNR	17.98	23.16	21.61	23.59	23.46	23.64	23.78
	SSIM	57.49	83.23	78.35	85.92	84.82	85.73	86.12
img17	PSNR	16.14	23.33	22.85	25.78	24.77	25.59	25.71
	SSIM	50.31	82.86	81.20	89.64	85.57	88.60	89.18
img1	PSNR	18.27	24.85	22.71	25.85	25.21	25.60	25.79
	SSIM	49.44	82.36	78.60	86.29	82.95	85.27	85.91
img2	PSNR	16.42	21.22	19.31	21.62	21.47	21.68	21.92
	SSIM	30.82	71.09	64.25	75.47	70.52	74.35	76.11
img3	PSNR	15.73	22.31	21.04	24.54	23.63	24.69	24.86
	SSIM	22.72	80.27	76.66	85.38	75.20	83.02	84.61
img4	PSNR	18.09	24.98	21.42	25.39	25.07	25.35	25.40
	SSIM	46.27	84.18	75.21	86.23	83.01	85.42	85.88
img5	PSNR	18.76	26.36	24.68	26.98	26.20	26.62	26.61
	SSIM	44.68	80.61	75.97	83.36	79.69	81.96	82.13
img6	PSNR	18.58	25.45	22.17	26.51	25.63	25.97	26.18
	SSIM	23.74	63.22	56.37	69.43	63.46	67.10	67.86
img7	PSNR	18.80	24.63	21.90	25.94	25.39	25.86	26.11
	SSIM	19.44	62.14	56.89	82.22	70.33	78.30	80.50
img8	PSNR	18.13	24.95	21.98	25.59	25.27	25.61	25.69
	SSIM	58.72	89.53	84.72	92.06	89.88	91.42	91.78
img9	PSNR	19.04	26.52	23.32	27.78	26.93	27.40	27.58
	SSIM	65.57	91.88	87.84	94.97	91.97	93.96	94.49
Ave.	PSNR	18.21	25.56	22.86	26.25	25.51	26.03	26.22
	SSIM	51.49	83.76	79.47	87.94	84.15	86.81	87.50